Extracted from "Quantum Phase Transitions", S. Sachdev, Cambridge University Press (1999)

13

Heisenberg spins: ferromagnets and antiferromagnets

Part 2 of this book dealt with the magnetically ordered and quantum paramagnetic phases of models of N-component quantum rotors. In Chapter 10 we showed how the $N = 2$ rotors could be mapped onto certain boson models in the vicinity of a phase transition between a Mott insulator and a superfluid. In this chapter we shall consider models of Heisenberg spins: these directly represent the spin fluctuations of physical electrons in insulators or other systems with an energy gap towards charged excitations (*e.g.,* certain quantum Hall states). We shall describe the conditions under which certain models of Heisenberg spins reduce to $N = 3$ quantum rotor models, thus providing the long-promised physical motivation for studying the latter models; recall that a preview of this mapping already appeared in Section 5.1.1.1. We shall also discuss the physical properties of Heisenberg spin models under conditions in which they do not map onto the rotor models of Part 2.

We will deal with lattice models with the Hamiltonian

$$H_S = -\sum_{i,j} J_{ij} \hat{\mathbf{S}}_i \cdot \hat{\mathbf{S}}_j - \mathbf{H} \cdot \sum_i \hat{\mathbf{S}}_i. \tag{13.1}$$

Here the magnetic field $\mathbf{H}$ is precisely the same (with no overall scale factor) as that appearing in the rotor Hamiltonian (5.1): $\mathbf{H}$ couples to a conserved total spin (or for the rotors the total angular momentum) which, as we will see, commutes with the rest of the Hamiltonian. The $\hat{\mathbf{S}}_i$ are Heisenberg spin operators whose basic properties were introduced in Section 5.1.1.1: they satisfy the commutation relations (5.8) on each site i, and act on the $2S+1$ states (5.9) of the spin S representation on each site. The J_{ij} are a set of translationally-invariant exchange interactions between these sites.

We will begin in Section 13.1 by showing how to set up a path integral

for systems with states restricted in the manner (5.9,5.10) on each site. Then Section 13.2 will consider the properties of *ferromagnets* in which all $J_{ij} > 0$, and the ground state is the fully polarized state with all spins parallel and the total spin takes its maximum possible value. The properties of antiferromagnets in which the ground state has negligible total spin will be discussed in Section 13.3–these are likely to arise when all $J_{ij} < 0$. Finally Section 13.4 will consider more complex situations with partial uniform polarization of the spins, which is accompanied by a certain 'canted' order in dimensions $d > 1$.

13.1 Coherent state path integral

We have previously encountered the coherent state path integral in Section 10.2 where we introduced, following Refs [385, 486], a path integral representation of canonical bosons. An important feature of the path integral was the 'Berry phase' term $b^\dagger db/d\tau$ in (10.19) which accounted for the kinematics of ordinary bosons, and played an important role in the structure of the Mott insulating phases and the nature of their transitions to the superfluid. In this section we will present a reasonably complete derivation of the corresponding path integral for the quantum mechanics of the spin states (5.9). Many derivations of this path integral exist in the literature, but we shall follow here the approach used in Ref [425] which has the advantage of explicitly maintaining spin rotation invariance. The reader is also referred to a collection of reprints [300] for further information on coherent states and their relationship to path integrals.

We shall deal in this section with a single Heisenberg spin, and will therefore drop the site index. There is no loss of generality in this, as the same manipulations can be carried out independently on each site. The derivation of any path integral proceeds by the insertion of a complete set of states at infinitesimal intervals in time upon the time evolution operator of the system. It would clearly pay to choose a set of states under which the matrix elements of $\hat{\mathbf{S}}$ are simple: for this reason the states in (5.9) are not convenient. Instead, we shall use the so-called spin-coherent states. These are an infinite set of states $|\mathbf{N}\rangle$, labeled by the points $\mathbf{N}$ on the surface of the unit sphere; so $\mathbf{N}$ is a three-component vector satisfying $\mathbf{N}^2 = 1$. As there are only a total of $2S+1$ independent states, these states clearly cannot be mutually orthogonal.

They are normalized to unity

$$\langle \mathbf{N}|\mathbf{N}\rangle = 1, \tag{13.2}$$

$\langle \mathbf{N}|\mathbf{N}'\rangle \neq 0$ for $\mathbf{N} \neq \mathbf{N}'$, and satisfy the completeness relation

$$\int \frac{d\mathbf{N}}{2\pi} |\mathbf{N}\rangle\langle \mathbf{N}| = 1 = \sum_{m=-S}^{S} |S,m\rangle\langle S,m|, \tag{13.3}$$

where the integral of $\mathbf{N}$ is over the unit sphere. Because of their non-orthogonality, these states are called 'over-complete'. What makes them extremely useful is that the diagonal expectation value of the operator $\hat{\mathbf{S}}$ is very simple:

$$\langle \mathbf{N}|\hat{\mathbf{S}}|\mathbf{N}\rangle = S\mathbf{N}. \tag{13.4}$$

So the state $|\mathbf{N}\rangle$ is almost like a classical spin of length S pointing in the $\mathbf{N}$ direction; indeed, the spin coherent states are the minimum uncertainty states localized as much in the $\mathbf{N}$ direction as the principles of quantum mechanics will allow, and in the large S limit, $|\mathbf{N}\rangle$ reduces to a classical spin in the $\mathbf{N}$ direction.

The relations (13.2), (13.3), and (13.4) define the spin coherent states. Let us explicitly construct them. For $\mathbf{N} = (0,0,1)$, the state $|\mathbf{N}\rangle$ is easy to determine; we have

$$|\mathbf{N} = (0,0,1)\rangle = |S, m = S\rangle \equiv |\Psi_0\rangle \tag{13.5}$$

We have labeled this particular coherent state as a reference state $|\Psi_0\rangle$ as it will be needed frequently in the following. Now it should be clear that for other values of $\mathbf{N}$ we can obtain $|\mathbf{N}\rangle$ simply by acting on $|\Psi_0\rangle$ by an operator which performs a $SU(2)$ rotation from the direction $(0,0,1)$ to the direction $\mathbf{N}$. In this manner we obtain the following explicit representation for the coherent state $|\mathbf{N}\rangle$

$$|\mathbf{N}\rangle = \exp\left(z\hat{S}_+ - z^*\hat{S}_-\right)|\Psi_0\rangle \tag{13.6}$$

where the complex number z is related to the vector $\mathbf{N}$. This relationship is simplest in spherical co-ordinates; if we parameterize $\mathbf{N}$ as

$$\mathbf{N} = (\sin\theta\cos\phi, \sin\theta\sin\phi, \cos\theta) \tag{13.7}$$

then

$$z = -\frac{\theta}{2}\exp(-i\phi). \tag{13.8}$$

We leave it as an exercise for the reader to verify that (13.6) satisfies

(13.2), (13.3) and (13.4); this verification is aided by the knowledge that the value of the expression $\exp(-i\mathbf{a}\cdot\hat{\mathbf{S}})\hat{\mathbf{S}}\exp(i\mathbf{a}\cdot\hat{\mathbf{S}})$, where $\mathbf{a}$ is some vector, is determined solely by the spin commutation relations (5.8), and can therefore be worked out by temporarily assuming that the $\hat{\mathbf{S}}$ are twice the Pauli matrices–the result, when expressed in terms of $\hat{\mathbf{S}}$, is valid for arbitrary S.

It will be useful for our subsequent formulation to rewrite the above results in a somewhat different manner, making the $SU(2)$ symmetry more manifest. Define the 2×2 matrix of operators $\hat{\mathcal{S}}$ by

$$\hat{\mathcal{S}} = \begin{pmatrix} \hat{S}_z & \hat{S}_x - i\hat{S}_y \\ \hat{S}_x + i\hat{S}_y & -\hat{S}_z \end{pmatrix}. \tag{13.9}$$

Then Eqn. (13.5) can be rewritten as

$$\langle \mathbf{N}|\hat{\mathcal{S}}_{\alpha\beta}|\mathbf{N}\rangle = SW_{\alpha\beta}, \tag{13.10}$$

where the matrix W is

$$W = \begin{pmatrix} N_z & N_x - iN_y \\ N_x + iN_y & -N_z \end{pmatrix} \equiv \mathbf{N}\cdot\vec{\sigma} \tag{13.11}$$

where $\vec{\sigma}$ are the Pauli matrices. So instead of labeling the coherent states with the unit vector $\mathbf{N}$, we could equally well use the traceless Hermitean matrix W. Furthermore, there is a simple relationship between W and the complex number z. In particular, if we use the spin-1/2 version of the operator in Eqn. (13.6)

$$U = \exp\left[\begin{pmatrix} 0 & z \\ -z^* & 0 \end{pmatrix}\right] \tag{13.12}$$

(U is thus a 2×2 matrix), then we find

$$W = U\sigma_z U^\dagger \tag{13.13}$$

We proceed to the derivation of the coherent state path integral for the partition function

$$Z = \mathrm{Tr}\exp(-H(\hat{\mathbf{S}})/T); \tag{13.14}$$

we will restrict the following discussion to Hamiltonians in which H is a linear function of any given $\hat{\mathbf{S}}$ on a fixed site. The H in Eqn. (13.1) is certainly of this type. The transformation of Z into a path-integral proceeds along the same lines as that discussed in Refs [385, 486] for

bosons. We break up the exponential into a large number of exponentials of infinitesimal time evolution operators

$$Z = \lim_{M\to\infty} \prod_{i=1}^{M} \exp(-\Delta\tau_i H(\hat{\mathbf{S}})), \tag{13.15}$$

where $\Delta\tau_i = 1/MT$, and insert a set of coherent states between each exponential by using the identity (13.3); we label the state inserted at a 'time' τ by $|\mathbf{N}(\tau)\rangle$. We can then evaluate the expectation value of each exponential by use of the identity (13.4)

$$\begin{aligned}
&\langle \mathbf{N}(\tau)| \exp(-\Delta\tau H(\hat{\mathbf{S}}))|\mathbf{N}(\tau+\Delta\tau)\rangle \\
&\quad \approx \langle \mathbf{N}(\tau)|1 - \Delta\tau H(\hat{\mathbf{S}})|\mathbf{N}(\tau+\Delta\tau)\rangle \\
&\quad \approx 1 - \Delta\tau \langle \mathbf{N}(\tau)|\frac{d}{d\tau}|\mathbf{N}(\tau)\rangle - \Delta\tau H(S\mathbf{N}) \\
&\quad \approx \exp\left(-\Delta\tau \langle \mathbf{N}(\tau)|\frac{d}{d\tau}|\mathbf{N}(\tau)\rangle - \Delta\tau H(S\mathbf{N})\right).
\end{aligned} \tag{13.16}$$

In each step we have retained expressions correct to order $\Delta\tau$. The coherent states at time τ and $\tau+\Delta\tau$ can in principle have completely different orientations, so, a priori, it is not clear that expanding these states in derivatives of time is a valid procedure. This is a subtlety that afflicts all coherent state path integrals, and has been discussed more carefully by Negele and Orland [385]: the conclusion of their analysis is that except for the single 'tadpole' diagram where a point-splitting of time becomes necessary, this expansion in derivatives of time always leads to correct results. In any case, the resulting coherent state path integral is a formal expression which cannot be directly evaluated, and in case of any doubt one should always return to the original discrete time product in (13.15).

Keeping in mind the above caution, we insert (13.16) into (13.15), take the limit of small $\Delta\tau$ and obtain the following functional integral for Z

$$Z = \int_{\mathbf{N}(0)=\mathbf{N}(1/T)} \mathcal{D}\mathbf{N}(\tau) \exp\left\{-\int_0^{1/T} d\tau \left[\mathcal{S}_B + H(S\mathbf{N}(\tau))\right]\right\}, \tag{13.17}$$

where

$$\mathcal{S}_B = \langle \mathbf{N}(\tau)|\frac{d}{d\tau}|\mathbf{N}(\tau)\rangle \tag{13.18}$$

and $H(S\mathbf{N})$ is obtained by replacing every occurrence of $\hat{\mathbf{S}}$ in the Hamiltonian by $S\mathbf{N}$. The promised Berry phase term is S_B, and it represents

the overlap between the coherent states at two infinitesimally separated times. It can be shown straightforwardly from the normalization condition, $\langle \mathbf{N}|\mathbf{N}\rangle = 1$, that $\mathcal{S}_B$ is pure imaginary. In the remainder of this section we will manipulate $\mathcal{S}_B$ into a physically more transparent form using the expressions above for the coherent states. For the case of the boson coherent state path integral, it is precisely the analog of $\mathcal{S}_B$ which becomes $b^\dagger(\partial b/\partial\tau)$ in (10.19).

Clearly, the τ-dependence of $\mathbf{N}(\tau)$ implies a τ dependent $z(\tau)$ through (13.8). From (13.6) we have therefore

$$\frac{d}{d\tau}|\mathbf{N}(\tau)\rangle = \frac{d}{d\tau}\exp\left(z(\tau)\hat{S}_+ - z^*(\tau)\hat{S}_-\right)|\Psi_0\rangle \tag{13.19}$$

Taking this derivative is however not so simple: notice that if an operator $\hat{O}$ does not commute with its derivative $d\hat{O}/d\tau$ then

$$\frac{d}{d\tau}\exp(\hat{O}) \neq \frac{d\hat{O}}{d\tau}\exp(\hat{O}) \tag{13.20}$$

The correct form of this result is in fact

$$\frac{d}{d\tau}\exp(\hat{O}) = \int_0^1 du \exp(\hat{O}(1-u))\frac{d\hat{O}}{d\tau}\exp(\hat{O}u), \tag{13.21}$$

where u is just a dummy integration variable. This result can be checked by expanding both sides in powers of $\hat{O}$ and verifying that they agree term by term. More constructively, a 'hand-waving' derivation can be given as follows

$$\begin{aligned}
\frac{d}{d\tau}\exp(\hat{O}) &= \frac{d}{d\tau}\exp\left(\hat{O}\int_0^1 du\right) \\
&= \lim_{M\to\infty}\frac{d}{d\tau}\exp\left(\sum_{i=1}^{M}\hat{O}\Delta u_i\right) \quad \text{with } \Delta u_i = 1/M \\
&\approx \lim_{M\to\infty}\frac{d}{d\tau}\prod_{i=1}^{M}\exp\left(\hat{O}\Delta u_i\right) \\
&\approx \lim_{M\to\infty}\sum_{j=1}^{M}\prod_{i=1}^{j}\exp\left(\hat{O}\Delta u_i\right)\frac{d\hat{O}}{d\tau}\Delta u_j\prod_{i=j+1}^{M}\exp\left(\hat{O}\Delta u_i\right)
\end{aligned} \tag{13.22}$$

Finally, taking the limit $M\to\infty$, we obtain the needed result (13.21). Now using (13.19) and (13.21) we find

$$\mathcal{S}_B = \int_0^{1/T} d\tau \langle \mathbf{N}(\tau)|\frac{d}{d\tau}|\mathbf{N}(\tau)\rangle$$

$$= \int_0^{1/T} d\tau \int_0^1 du \langle \mathbf{N}(\tau,u)| \left(\frac{\partial z}{\partial \tau}\hat{S}_+ - \frac{\partial z^*}{\partial \tau}\hat{S}_- \right) |\mathbf{N}(\tau,u)\rangle \quad (13.23)$$

where $\mathbf{N}(\tau,u)$ is defined by

$$|\mathbf{N}(\tau,u)\rangle = \exp\left(u \left(z(\tau)\hat{S}_+ - z^*(\tau)\hat{S}_- \right) \right) |\Psi_0\rangle \quad (13.24)$$

From this definition, three important properties of $\mathbf{N}(\tau,u)$ should be apparent

$$\begin{aligned} &\mathbf{N}(\tau,u=1) \equiv \mathbf{N}(\tau), \\ &\mathbf{N}(\tau,u=0) = (0,0,1), \\ \text{and } &\mathbf{N}(\tau,u) \text{ moves with } u \text{ along the great circle} \\ &\text{between } \mathbf{N}(\tau,u=0) \text{ and } \mathbf{N}(\tau,u=1) \end{aligned} \quad (13.25)$$

We can visualize the dependence on u by imagining a *string* connecting the physical value of $\mathbf{N}(\tau) = \mathbf{N}(\tau,u=1)$ to the North pole, along which u decreases to 0. Associated with each $\mathbf{N}(\tau,u)$ we can also define a u-dependent $W(\tau,u)$ as in Eqn. (13.11); the analog of (13.25) is $W(\tau,u=1) \equiv W(\tau)$ and $W(\tau,u=1) = \sigma_z$. A simple explicit expression for $W(\tau,u)$ is also possible: we simply generalize (13.12) to

$$U(\tau,u) = \exp\left[u \begin{pmatrix} 0 & z \\ -z^* & 0 \end{pmatrix} \right] \quad (13.26)$$

then the relationship (13.13) gives us $W(\tau,u)$. Now we can use the expression (13.10) to rewrite (13.23) as

$$\mathcal{S}_B = S \int_0^{1/T} d\tau \int_0^1 du \left[\frac{\partial z}{\partial \tau} W_{21}(\tau,u) - \frac{\partial z^*}{\partial \tau} W_{12}(\tau,u) \right], \quad (13.27)$$

As everything is a periodic function of τ, we may freely integrate this expression by parts and obtain

$$\mathcal{S}_B = -S \int_0^{1/T} d\tau \int_0^1 du \mathrm{Tr}\left[\begin{pmatrix} 0 & z(\tau) \\ -z^*(\tau) & 0 \end{pmatrix} \partial_\tau W(\tau,u) \right]. \quad (13.28)$$

where the trace is over the 2×2 matrix indices. The definitions (13.13) and (13.26) can be used to easily establish the identity

$$\begin{pmatrix} 0 & z(\tau) \\ -z^*(\tau) & 0 \end{pmatrix} = -\frac{1}{2} W(\tau,u) \frac{\partial W(\tau,u)}{\partial u}, \quad (13.29)$$

which when inserted into (13.28) yields the expression for $\mathcal{S}_B$ in one of

its final forms

$$\mathcal{S}_B = \int_0^{1/T} d\tau \int_0^1 du \left[\frac{S}{2} \mathrm{Tr} \left(W(\tau,u) \frac{\partial W(\tau,u)}{\partial u} \frac{\partial W(\tau,u)}{\partial \tau} \right) \right] \quad (13.30)$$

An expression for $\mathcal{S}_B$ solely in terms of $\mathbf{N}(\tau,u)$ can be obtained by substituting in (13.11); this yields the final expression for $\mathcal{S}_B$, which when inserted in (13.17) gives us the coherent state path integral for a spin:

$$\mathcal{S}_B = iS \int_0^{1/T} d\tau \int_0^1 du \; \mathbf{N} \cdot \left(\frac{\partial \mathbf{N}}{\partial u} \times \frac{\partial \mathbf{N}}{\partial \tau} \right) \quad (13.31)$$

This expression has a simple geometric interpretation. The function $\mathbf{N}(\tau,u)$ is a map from the rectangle $0 \leq \tau \leq 1/T$, $0 \leq u \leq 1$ to the unit sphere. As $\mathbf{N}$ moves from $\mathbf{N}(\tau)$ to $\mathbf{N}(\tau+\Delta\tau)$ it drags along the string connecting it to the North pole represented by the u dependence of $\mathbf{N}(\tau,u)$ (recall (13.25)). It is easy to see that the contribution to $\mathcal{S}_B$ of this evolution is simply iS times the oriented area swept out by the string. The value of this area clearly depends upon the fact that $u=0$ end of the string was pinned at the North pole: this was a 'gauge' choice, and by choosing the phases of the coherent states differently, we could have pinned the point $u=0$ anywhere on the sphere. However when we consider the complete integral over τ in (13.31), the boundary condition $\mathbf{N}(1/T) = \mathbf{N}(0)$ (required by the trace in (13.14) shows that $\mathbf{N}(\tau)$ sweeps out a closed loop on the unit sphere. Then the total τ integral in (13.31) is the area contained within this loop, and is independent of the choice of the location of the $u=0$ point. Actually this last statement is not completely correct: the 'inside' of a closed loop is not well-defined and the location of the $u=0$ point makes the oriented area uncertain modulo 4π (which is the total area of the unit sphere). So the net contribution of $e^{\mathcal{S}_B}$ is uncertain up to a factor of $e^{i4\pi S}$. For consistency, we can now demand that this arbitrary factor always equal unity, which, of course, leads to the familiar requirement that $2S$ be an integer.

13.2 Quantized ferromagnets

We turn to the lattice model H_S in (13.1), and consider the case of ferromagnetic interactions where all $J_{ij} > 0$. In this case, the state with all spins parallel $\prod_i |S,S\rangle_i$ is the exact ground state (see, *e.g.,* Ref. [28]; we have assumed that the field $\mathbf{H}$ points along the spin quantization z axis). The adjective 'quantized' in the title refers to the fact that the

magnetization density, M_0, (this is magnitude of the expectation value of the total spin magnetization $\sum_i \hat{\mathbf{S}}_i$ divided by the system volume) is pinned at a simple value which can be determined a priori, and which does *not* vary as the exchange constants J_{ij} are varied. In Section 13.4, we will meet examples of quantized ferromagnets in which the magnetic moment is quantized, but not at a fully polarized value: fractional quantization is also possible, but in every case twice the average total spin moment per unit cell is an integer. The discussion in this chapter will apply to the low energy properties of all such quantized ferromagnets, but will only explicitly refer to the fully polarized case.

Apart from their quantized moment, the characteristic property of a quantized ferromagnet is that the only low-lying excitation which carries spin is a 'spin-wave' which arises from a slow rotation of the orientation of the ordered moment. Many readers may be familiar with the fact that the wave function of a single spin-wave excitation can also be written down exactly for a fully polarized, quantized ferromagnet: these well-known results will also emerge below. The purpose of our discussion shall be two-fold: (*i*) to obtain a continuum field theory of the low-lying excitations of the quantized ferromagnet, and to understand its behavior under a scaling transformation, and (*ii*) to use the continuum theory to systematically enumerate the parameters required describe the low T properties of such ferromagnets.

We begin by constructing the continuum field theory for the low-lying excitations above the fully-polarized ferromagnetic ground state. It is reasonable to expect that these will consist of fluctuations in which the orientations of the spins varies slowly from site to site. We start with the functional integral like (13.17) for the spin orientation $\mathbf{N}_i(\tau)$ on each site i, and perform a gradient expansion by introducing the continuum field $\mathbf{N}(x,\tau)$. Keeping terms up to second spatial derivatives we obtain for the partition function $Z = \mathrm{Tr} e^{-H_S/T}$ [271]:

$$Z = \int \mathcal{D}\mathbf{N}(x,\tau)\delta(\mathbf{N}^2-1)\exp\left(-\int_0^{1/T} d\tau \int d^d x \mathcal{L}_F\right)$$
$$\mathcal{L}_F = iM_0\int_0^1 du \mathbf{N}\cdot\left(\frac{\partial \mathbf{N}}{\partial u}\times\frac{\partial \mathbf{N}}{\partial \tau}\right) - M_0\mathbf{N}\cdot\mathbf{H} + \frac{\rho_s}{2}(\nabla\mathbf{N})^2, \quad (13.32)$$

where $M_0 \equiv S/v$ is the magnetization density of the ground state, v is the volume per site, and ρ_s is the spin stiffness. We introduced the analogous stiffness for the rotor model in Section 5.3.3; here, the gradient

expansion upon the partition function of H_S gives us

$$\rho_s = \frac{S^2}{2v} \sum_m J_r x_{m1}^2, \tag{13.33}$$

where the J_m are the set of exchange constants coupling a given site i to the other sites separated from i by $(x_{m1}, x_{m2} \dots x_{md})$; the sum over m includes separate terms for $\vec{x}_m$ and $-\vec{x}_m$. The continuum theory (13.32) should really be regarded as a convenient schematic representation of the quantum ferromagnet, and we will often need to go back to the underlying lattice model H_S to regulate short distance singularities.

We consider the behavior of $\mathcal{L}_F$ under a rescaling transformation [429] at $T = 0$. The continuum theory is characterized by two dimensionful couplings M_0 and ρ_s, and despite the non-linear constraint in (13.32), some special properties of the quantum theory make it possible to determine their exact renormalization group flow equations (this should be contrasted from the rotor theory (5.16) where no such exact results were available). First, we noticed at the end of Section 13.1 that the single spin Berry phase was uncertain up to an additive constant of $4\pi S$, and this imposed the requirement that S be integer or half-integer. Precisely the same argument applied to the Berry phase of the continuum ferromagnet (13.32) in a hypercubic box of volume L^d, implies $2M_0L^d$ must be an integer (this is just a fancy way of saying that the continuum ferromagnet must model an integral number of spins). This integer cannot change under any scaling transformation, and as L transform as a physical length, the invariance of M_0L^d leads to the exact flow equation

$$\frac{dM_0}{d\ell} = dM_0. \tag{13.34}$$

This equation describes the quantization of the average magnetic moment at its fully saturated value.

A closely related scaling equation holds for ρ_s, and this follows from the exactly known single spin-wave spectrum. To prepare for some future computations, we derive this by going back to the lattice Hamiltonian, H_S, and then taking the continuum limit of the resulting response functions. The most convenient formalism for computations is provided by the Dyson-Maleev transformation [140, 349] from the spin operators $\hat{\mathbf{S}}_i$ to Bose operators $\hat{b}_i$. Explicitly, the mapping is

$$\begin{aligned} \hat{S}_{+i} &= \sqrt{2S}\hat{b}_i^\dagger \\ \hat{S}_{-i} &= \sqrt{2S}\left(\hat{b}_i - \frac{1}{2S}\hat{b}_i^\dagger \hat{b}_i \hat{b}_i\right) \end{aligned}$$

$$\hat{S}_z = -S + \hat{b}_i^\dagger \hat{b}_i. \tag{13.35}$$

Along with the constraint $\hat{b}_i^\dagger \hat{b}_i \leq 2S$, this defines an exact mapping between the Hilbert space of the spin S spins ($2S+1$ states per spin) and the bosons ($2S+1$ possible boson occupation numbers); in practice, one does not even have to impose the constraint $\hat{b}_i^\dagger \hat{b}_i \leq 2S$, as all matrix elements out of the physical sector vanish. The reader can verify that the operators in (13.35) do indeed satisfy the commutation relations (5.8). The relations (13.35) do not satisfy the hermiticity requirement $\hat{S}_{+i} = (\hat{S}_{-i})^\dagger$, but this can be repaired by performing a similarity transformation on the space of spin states: the reader should consult Ref [16] for more information, as here we shall mainly use (13.35) as a black-box tool. Inserting (13.35) into (13.1), and Fourier transforming to momentum space by defining $\hat{b}(\vec{k}) = \sqrt{v}\sum_i \hat{b}_i e^{-i\vec{k}\cdot\vec{x}}$ (these Bose operators then satisfy the canonical continuum commutation relations $[\hat{b}(\vec{k}), \hat{b}^\dagger(\vec{k}')] = (2\pi)^3\delta^d(\vec{k}-\vec{k}')$), the Hamiltonian becomes

$$H_S = \int \frac{d^dk}{(2\pi)^d}\left\{S\left[J(0) - J(\vec{k})\right] + H\right\}\hat{b}^\dagger(\vec{k})\hat{b}(\vec{k}) +$$
$$\frac{v}{2}\int\prod_{i=1}^{4}\frac{d^dk_i}{(2\pi)^d}(2\pi)^d\delta^d(\vec{k}_1+\vec{k}_2-\vec{k}_3-\vec{k}_4)\left[J(\vec{k}_1) - J(\vec{k}_1-\vec{k}_4)\right]$$
$$\times\hat{b}^\dagger(\vec{k}_1)\hat{b}^\dagger(\vec{k}_2)\hat{b}(\vec{k}_3)\hat{b}(\vec{k}_4) \tag{13.36}$$

where all momentum integrals are over the first Brillouin zone of the lattice, and

$$J(\vec{k}) = \sum_m J_m e^{-i\vec{k}\cdot\vec{x}_m}. \tag{13.37}$$

This bosonic form for H_S can be analyzed by the methods developed in Chapter 11 for (11.1). The ground state is the vacuum, $|0\rangle$, with no $\hat{b}$ particles (the fully polarized ferromagnet), while the lowest excitations are single boson states, $\hat{b}^\dagger(\vec{k})|0\rangle$, ('spin waves') which are exact eigenstates of H_S with energy $\varepsilon_{\vec{k}} = S(J(0) - J(\vec{k}) + H$. We have $\varepsilon_{\vec{k}} > 0$ for all $\vec{k}$, which indicates that the choice of the no boson state as the ground state is a consistent one. At $T = 0$, the one particle propagator is given exactly by the free particle propagator, as in (11.50), for there are no other particles present. Taking the small momentum limit of this propagator, and using the correspondence between the continuum fields

$$\hat{b}^\dagger(\vec{k}, \omega_n) = (M_0/2)^{1/2} N_+(-\vec{k}, -\omega_n) \tag{13.38}$$

which follows from our definitions above ($N_\pm = N_x \pm iN_y$), we obtain

an exact result for a two-point correlator of (13.32)

$$\left\langle N_-(-\vec{k},-\omega_n)N_+(\vec{k},\omega_n)\right\rangle = \frac{2}{-i\omega_n M_0+\rho_s k^2+M_0 H}. \qquad (13.39)$$

This represents the propagation of spin waves with the exact dispersion $\varepsilon_k = (\rho_s/M_0)k^2 + H$. The consistency of this dispersion with the scaling transformation requires $\dim[H] = z$ (as before in (5.42)), and the exact scaling equation

$$\frac{d\rho_s}{d\ell} = (d+z-2)\rho_s. \qquad (13.40)$$

As the spin-wave disperses quadratically with momentum at small k, it is convenient to choose $z = 2$ (other choices are also permissible, as physical observables will have compensating scale dependence arising from that of ρ_s).

The exact results (13.34), (13.39) and (13.40) are strongly reminiscent of the behavior of the Bose gas in Section 11.8. In both cases, the simplicity is due to the fluctuationless nature of the ground state and the exactly known single particle excitations. For the case of the Bose gas we had an additional non-linearity u, whose renormalization was determined by examining the two-particle scattering amplitude. In the present situation, the dimensionful parameters ρ_s and M_0 determine both the single particle dispersion (13.39) and the strengths of the non-linear couplings. It might therefore seem that the finite T properties of (13.32) must be given by universal functions of T, and the *bare* couplings ρ_s and M_0, consistent with the requirements of scaling and engineering dimensional analysis. However, this will be only the case if a short distance cutoff scale (explicitly present in (13.36) but not in (13.32)) did not influence the low energy properties. Such a scale might be required to cut-off large momentum (ultraviolet) divergences of momentum integrals over virtual excitations. Motivated by the structure of the Bose gas problem in Section 11.3, we look for ultraviolet divergences in the two spin-wave scattering amplitude at $T = 0$ (we need not consider $T > 0$ explicitly as the finite T corrections all involve Bose functions which fall off exponentially at large momentum). For the Bose gas problem we found ultraviolet divergences for $d \geq 2$, and this identified $d = 2$ as the upper critical dimension below which the universality of the continuum theory was robust. We will compute the on-shell T matrix of two spin waves coming in with momenta $\vec{k}_1$ and $\vec{k}_2$, and scattering into spin waves with momenta $\vec{k}_1 + \vec{q}$ and $\vec{k}_2 - \vec{q}$. Conservation of energy requires

$$J(\vec{k}_1) + J(\vec{k}_2) = J(\vec{k}_1 + \vec{q}) + J(\vec{k}_2 - \vec{q}). \qquad (13.41)$$

To zeroth order in $1/S$, the Hamiltonian (13.36) gives us the bare T-matrix element $v[J(\vec{k}_1+\vec{q})+J(\vec{k}_2-\vec{q})-J(\vec{k}_1+\vec{q}-\vec{k}_2)-J(\vec{q})]$. The first order in $1/S$ correction to the T-matrix is given by the first diagram in Fig 11.3, and by standard quantum mechanical perturbation theory [521], it evaluates to (this expression is the analog of (11.44))

$$\frac{v^2}{S}\int \frac{d^dq_1}{(2\pi)^d}[J(\vec{k}_1+\vec{q}_1)+J(\vec{k}_2-\vec{q}_1)-J(\vec{k}_1+\vec{q}_1-\vec{k}_2)-J(\vec{q}_1)]$$
$$\times[J(\vec{k}_1+\vec{q})+J(\vec{k}_2-\vec{q})-J(\vec{k}_1+\vec{q}-\vec{k}_2+\vec{q}_1)-J(\vec{q}-\vec{q}_1)]$$
$$\frac{}{J(\vec{k}_1)+J(\vec{k}_2)-J(\vec{k}_1+\vec{q}_1)-J(\vec{k}_2-\vec{q}_1)}. \quad (13.42)$$

To understand the implications of this result for the continuum theory (13.32) we allow the external momenta $\vec{k}_1$, $\vec{k}_2$, $\vec{q}$ to become small, but for the moment allow the internal momentum $\vec{q}_1$ to be large. Then there is a term from (13.42) which is quadratic in external momenta; however this can be seen to vanish after use of the identity $\int d^dq_1 e^{-i\vec{q}_1\cdot\vec{x}_m}=0$ (valid because all the $\vec{x}_m\neq 0$)–it is clear that the lattice regularization is crucial in obtaining this result, and it turns out that it is mainly this step which cannot be deduced from the continuum theory (13.32). The next term is *quartic* in external momenta, and it simplifies to

$$\frac{v^2}{S}\int \frac{d^dq_1}{(2\pi)^d}\frac{\left[\sum_m J_m e^{-i\vec{q}_1\cdot\vec{x}_m}(\vec{k}_1\cdot\vec{x}_m)(\vec{k}_2\cdot\vec{x}_m)\right]^2}{\sum_m J_m(1-e^{-i\vec{q}_1\cdot\vec{x}_m})}; \quad (13.43)$$

We take the small $\vec{q}_1$ limit of (13.43) and obtain the result for the correction to the two spin-wave T-matrix [307] at low momenta:

$$\frac{4\rho_s}{M_0^3}(\vec{k}_1\cdot\vec{k}_2)^2\int\frac{d^dq_1}{(2\pi)^d}\frac{1}{q_1^2}; \quad (13.44)$$

this expression involves only couplings present in $\mathcal{L}_F$ in (13.32) and so could also have been obtained directly from the continuum quantum theory after ignoring ultraviolet divergences in terms lower order in the external momenta. The integral in (13.44) is dominated by the ultraviolet for $d>2$ and so we have to return to the lattice expression (13.43). However it is ultraviolet finite for $d<2$, and the continuum theory is insensitive to lattice perturbations; the infrared divergence will of course be cutoff by the external momenta, which have not been kept in the propagator in the above approximation. So as in the case of the dilute Bose gas in Section 11.3, we see the emergence of $d=2$ as a critical dimension.

It is very useful to interpret (13.44) in renormalization group sense.

If we imagine we are integrating out virtual spin wave fluctuations between momentum scales Λ and $\Lambda e^{-\ell}$ (Λ is a momentum cutoff), then these become the boundaries of the integration in (13.44), and the result generates a four gradient term to $\mathcal{L}_F$. The generated term cannot be quadratic in $\mathbf{N}$, as that would modify the exactly known spin wave dispersion. The simplest terms which modify *only* the two spin-wave scattering amplitude are quartic also in $\mathbf{N}$; by noting the momentum dependence on (13.44), using the low momentum limit of the energy conservation equation (13.41), and imposing the restrictions of rotation invariance of rotational invariance, a simple analysis shows that the generated term is [429]

$$\mathcal{L}_F \to \mathcal{L}_F + \lambda(\nabla_a N_\alpha \nabla_a N_\alpha \nabla_b N_\beta \nabla_b N_\beta - 2\nabla_a N_\alpha \nabla_b N_\alpha \nabla_a N_\beta \nabla_b N_\beta), \tag{13.45}$$

where λ is a *new* coupling constant of the continuum theory. Converting from scattering amplitudes of b to $\mathbf{N}$ quanta using (13.38), (13.45) and (13.44) imply the flow equation

$$\frac{d\lambda}{d\ell} = (d-2)\lambda + \frac{\rho_s}{M_0}. \tag{13.46}$$

As with (11.47), this flow equation is believed to be exact. So for $d < 2$, λ is attracted to a universal critical value, and the parameters ρ_s and M_0 completely determine the low energy physics of the continuum theory (13.32). On the other hand, λ becomes large at long distances for $d \geq 2$, and its bare value is important: it is responsible for temperature dependent corrections to the magnetization computed by Dyson [140].

For $d < 2$ these considerations imply that we may write down universal scaling forms for the continuum ferromagnet (13.32). The usual scaling and dimensional considerations imply for the free energy density [429]

$$\mathcal{F} \asymp T M_0 \Phi_{fm}\left(\frac{\rho_s}{M_0^{(d-2)/d}T}, \frac{H}{T}\right), \tag{13.47}$$

where Φ_{fm} is a universal function; corresponding results follow for observables which are derivatives of the free energy. Actually, our arguments for universality have really been made in an expansion in powers of $1/S$, and so the result (13.47) only holds as an asymptotic expansion in inverse powers of $\rho_s/(M_0^{(d-2)/d}T)$, and this represented by the symbol $\asymp$. Indeed, (13.47) is expected to be true to all orders in $\rho_s/(M_0^{(d-2)/d}T)$, but this is not the same thing as being exactly true. Lattice effects become significant when $T \sim \rho_s/M_0^{(d-2)/d}$, for then the

wavelength of the characteristic spin-wave is of order $M_0^{1/d}$, which is of order a lattice spacing; these effects appear as essential singularities and destroy strict equality for (13.47). Some short distance regularization at the scale $M_0^{1/d}$ is always required for any consistent theory of quantum ferromagnets [217]. Similar considerations apply for expansions in $1/N$ [27, 31, 524], and for ferromagnets with more complicated replica and supersymmetries [208, 209].

Finally, we briefly note that effective classical models for thermal fluctuations in ferromagnets can be derived for $T \ll \rho_s/M_0^{(d-2)/d}$, precisely as was done for the rotor models in Part 2. In $d = 1$ we would get the effective theory (2.68) with $\xi = \rho_s/T$ [517], while in $d = 2$ we would obtain the model (7.8) [303] with a $\Lambda_{\overline{MS}}$ which can be computed from (13.36) by methods parallel to those in Section 7.1.1.

13.3 Antiferromagnets

This section will consider models H_S in (13.1) with all $J_{ij} < 0$. Classically (*i.e.,* in the limit $S \to \infty$), such models will minimize their energies by making nearest neighbor spins acquire an anti-parallel orientation. On bi-partite lattices (*i.e.,* lattices which can be split into two equivalent sublattices so that all nearest neighbors of any site on one sublattice belong to the other sublattice) with nearest neighbor interactions, the anti-parallel constraint is easy to satisfy: the spins simply point in opposite directions on the two sublattices. Notice that any pair of spins is either parallel or antiparallel, and so such an ordering is *collinear*. We will begin by exclusively considering quantum antiferromagnets whose classical ground state is collinear in Section 13.3.1: such an ordering is expected to be present at least over short distances in the quantum case. Non-collinear ordering arises on non-bipartite lattices or even on bipartite lattices with further neighbor interactions: such antiferromagnets are classically frustrated and possess ground states in which the spins are *coplanar* (as on the triangular lattice with nearest neighbor interactions), or in some rare cases, can even form structures which are three-dimensional in spin space. We will consider the non-collinear cases in Section 13.3.2.

13.3.1 Collinear order

For definiteness, we will begin by considering antiferromagnets on a d-dimensional hypercubic lattice with only a nearest neighbor exchange

$J_{ij} = -J < 0$; other collinear antiferromagnets can be treated in a similar manner. In the classical limit of large S, as noted above, the ground state has spins oriented in opposite directions on the two sublattices: this is the so-called Néel-ordered state. For smaller S this orientation should survive at least over a few lattice spacings, suggesting that a continuum description of the quantum antiferromagnet may be possible [218, 3, 4]. We therefore begin by introducing a parameterization of the unit length spin field $\mathbf{N}_i(\tau)$ which captures this local ordering. We write

$$\mathbf{N}_i(x,\tau) = \lambda_i \mathbf{n}(x_i,\tau))\sqrt{1-(a^d/S)^2\mathbf{L}^2(x_i,\tau)} + (a^d/S)\mathbf{L}(x_i,\tau), \quad (13.48)$$

where λ_i equals ± 1 on the two sublattices and a is the lattice spacing. The fields $\mathbf{n}(x_i)$ and $\mathbf{L}(x_i)$ parameterize the staggered and uniform components of the Heisenberg spins. The prefactor of a^d/S has been associated with $\mathbf{L}$ so that the spatial integral of $\mathbf{L}$ over any region is precisely the total magnetization inside it. Both fields are assumed to be slowly varying on the scale of a lattice spacing. This is certainly true as $S \to \infty$, and it is hoped that this assumption remains valid down to $S = 1/2$. So we will treat $\mathbf{n}(x,\tau)$ and $\mathbf{L}(x,\tau)$ as continuum quantum fields which can be expanded in spatial gradients over separations of order a. These continuum fields satisfy the constraints

$$\mathbf{n}^2 = 1 \quad , \quad \mathbf{n}\cdot\mathbf{L} = 0, \quad (13.49)$$

which combined with (13.48) imply that $\mathbf{N}_i^2 = 1$ is obeyed. Further, spins on nearby sites are expected to be predominantly antiparallel, so the uniform component $\mathbf{L}$ should be small; more precisely we have

$$\mathbf{L}^2 \ll S^2 a^{-2d}. \quad (13.50)$$

The field $\mathbf{n}(x,\tau)$ clearly plays the role of the order parameter associated with Néel ordering. Note that although $\mathbf{n}$ varies slowly on the scale of a lattice spacing, values of $\mathbf{n}$ on well separated points can be considerably different, leaving open the possibility of a quantum paramagnetic phase with no magnetic long range order. Magnetic Néel order requires that the time-average orientation of $\mathbf{n}(x,\tau)$ is correlated across the sample: whether this happens will be determined by the effective action for $\mathbf{n}$ fluctuations, which we will now derive.

We insert the decomposition (13.48) for $\mathbf{N}_i$ into $H_S(S\mathbf{N}_i(\tau))$ and expand the result in gradients, and in powers of $\mathbf{L}$. This yields

$$H_S = \int d^d x \left[\frac{JS^2a^{2-d}}{2}(\nabla_x \mathbf{n})^2 + dJa^d\mathbf{L}^2 - \mathbf{H}\cdot\mathbf{L}\right]$$

$$\equiv \quad \frac{1}{2}\int d^dx \ \left[\frac{Nc}{g}(\nabla_x \mathbf{n})^2 + \frac{cg}{N}\mathbf{L}^2 - \mathbf{H}\cdot\mathbf{L}\right]. \tag{13.51}$$

In the second equation we have introduced the couplings $c = 2\sqrt{d}JSa$ and $g = (N/S)2\sqrt{d}a^{d-1}$: the notation is suggestive and anticipates our eventual mapping of the present model to the rotor models in (3.12) and (5.16). In the present case $N = 3$, but we introduced a general factor of N for notational consistency with Part 2. If we had used a different form for H_S with modified short-range exchange interactions, the continuum limit of H would have been the same but with new values of g and c.

To complete the expression for the coherent state path-integral of the antiferromagnet in the continuum limit, we also need the expression for $\mathcal{S}_B$ in terms of $\mathbf{n}, \mathbf{L}$. We insert (13.48) into the (13.31) and retain terms up to linear order in $\mathbf{L}$: this yields

$$\begin{aligned}\mathcal{S}_B = \mathcal{S}'_B + i\int d^dx \int_0^{1/T} d\tau \int_0^1 du \Bigg[\mathbf{n}\cdot\left(\frac{\partial\mathbf{n}}{\partial u}\times\frac{\partial\mathbf{L}}{\partial\tau}\right) \\ + +\mathbf{n}\cdot\left(\frac{\partial\mathbf{L}}{\partial u}\times\frac{\partial\mathbf{n}}{\partial\tau}\right) + \mathbf{L}\cdot\left(\frac{\partial\mathbf{n}}{\partial u}\times\frac{\partial\mathbf{n}}{\partial\tau}\right)\Bigg]\end{aligned} \tag{13.52}$$

where

$$\mathcal{S}'_B = iS\sum_i \lambda_i \int_0^{1/T} d\tau \int_0^1 du \ \mathbf{n}(x_i)\cdot\left(\frac{\partial\mathbf{n}(x_i)}{\partial u}\times\frac{\partial\mathbf{n}(x_i)}{\partial\tau}\right) \tag{13.53}$$

The evaluation of $\mathcal{S}'_B$ in the continuum limit is a rather subtle matter, as the leading λ_i in (13.53) shows that it is the sum of terms which oscillate in sign on the two sublattices. The naive assumption would be that these oscillating terms just cancel out, and therefore $\mathcal{S}'_B = 0$ in the continuum limit. For some purposes this assumption is in fact adequate, but there are a number of important cases where $\mathcal{S}'_B$ is non-vanishing and is crucial for a complete understanding of the physics. We will postpone a careful evaluation of $\mathcal{S}'_B$ to the following subsections where we will consider its consequences in $d = 1$ and $d = 2$ separately. Let us first simplify the other terms in (13.52) a bit further.

We use the fact that the vectors $\mathbf{L}$, $\partial\mathbf{n}/\partial\tau$, $\partial\mathbf{n}/\partial u$ are all perpendicular to $\mathbf{n}$; hence, they lie in a plane and have a vanishing triple product:

$$\mathbf{L}\cdot\left(\frac{\partial\mathbf{n}}{\partial u}\times\frac{\partial\mathbf{n}}{\partial\tau}\right) = 0. \tag{13.54}$$

Using (13.54) in (13.52) we find

$$\mathcal{S}_B = \mathcal{S}'_B + i\int d^dx \int_0^{1/T} d\tau \int_0^1 du \left[\frac{\partial}{\partial\tau}\left(\mathbf{n}\cdot\left(\frac{\partial\mathbf{n}}{\partial u}\times\mathbf{L}\right)\right)\right.$$

$$+\frac{\partial}{\partial u}\left(\mathbf{n}\cdot\left(\mathbf{L}\times\frac{\partial\mathbf{n}}{\partial\tau}\right)\right)\Big] \tag{13.55}$$

The total τ derivative yields 0 after using the periodicity of the fields in τ, while the total u derivative yields a surface contribution at $u=1$. This gives finally

$$\mathcal{S}_B = \mathcal{S}'_B - i\int d^dx \int_0^{1/T} d\tau \mathbf{L}\cdot\left(\mathbf{n}\times\frac{\partial\mathbf{n}}{\partial\tau}\right) \tag{13.56}$$

Putting together (13.51) and (13.56) in (13.17) we obtain the following path-integral for the partition function of the antiferromagnet

$$\begin{aligned} Z &= \int \mathcal{D}\mathbf{n}\mathcal{D}\mathbf{L}\delta(\mathbf{n}^2-1)\delta(\mathbf{L}\cdot\mathbf{n})\exp(-\mathcal{S}'_B-\mathcal{S}'_n) \\ \mathcal{S}'_n &= \frac{1}{2}\int_0^{1/T} d\tau \int d^dx\Big[\frac{Nc}{g}(\nabla_x\mathbf{n})^2 \\ &\qquad +\frac{cg}{N}\mathbf{L}^2 - 2i\mathbf{L}\cdot\left(\mathbf{n}\times\frac{\partial\mathbf{n}}{\partial\tau}-i\mathbf{H}\right)\Big] \end{aligned} \tag{13.57}$$

The functional integral over $\mathbf{L}$ can be carried out explicitly (after imposing the constraint $\mathbf{L}\cdot\mathbf{n}=0$, *e.g.,* by adding a term $w(\mathbf{L}\cdot\mathbf{n})^2$ to the Hamiltonian, and taking the limit $w\to\infty$ after carrying out the integral) and we obtain the final result of this section [218, 3, 4]

$$\begin{aligned} Z &= \int \mathcal{D}\mathbf{n}\delta(\mathbf{n}^2-1)\exp(-\mathcal{S}'_B-\mathcal{S}_n) \\ \mathcal{S}_n &= \frac{N}{2cg}\int_0^{1/T} d\tau\int d^dx\ \left[c^2(\nabla_x\mathbf{n})^2+(\partial_\tau\mathbf{n}-i\mathbf{H}\times\mathbf{n})^2\right]. \end{aligned} \tag{13.58}$$

Note that $\mathcal{S}_n$ is identical to the rotor model action studied in (5.16). However, before we can carry over all the results of Part 2 here, we have to examine the consequences of $\mathcal{S}'_B$, and this will be done separately in the following two subsections in dimensions $d=1$ and $d=2$ respectively.

13.3.1.1 $d=1$

It is simpler to evaluate S'_B in $d=1$ by a geometric argument, rather than working directly with the formal expression (13.53). We have already argued below (13.31), that the contribution of each site i in (13.53) equals $\lambda_i S$ times the area on the unit sphere contained inside the close loop defined by the periodic time evolution of $\mathbf{n}(x_i,\tau)$: we define this area to equal $\mathcal{A}_i$. Let us examine the contribution of two neighboring sites, i and $i+1$, to $\mathcal{S}'_B$. The weight λ_i will have opposite signs on

these sites, and so the net contribution will be the difference of the areas. We can further assume that the order parameter field $\mathbf{n}(x_i)$ only varies slightly between i and $i+1$: under these conditions, and using the definition of an area element on the sphere, we have (after defining $\Delta\mathbf{n}(x_i) = \mathbf{n}(x_{i+1}) - \mathbf{n}(x_i)$)

$$\begin{aligned} \mathcal{A}_{i+1} - \mathcal{A}_i &\approx \int_0^{1/T} d\tau \mathbf{n}(x_i) \cdot \left(\Delta\mathbf{n}(x_i) \times \frac{\partial \mathbf{n}(x_i)}{\partial \tau} \right) \\ &\approx a \int d\tau \mathbf{n}(x_i) \cdot \left(\frac{\partial \mathbf{n}(x_i)}{\partial x_i} \times \frac{\partial \mathbf{n}(x_i)}{\partial \tau} \right) \end{aligned} \tag{13.59}$$

The summation in (13.53) can be carried out over pairs of sites: all terms are of the same sign and therefore the summation can be easily converted into an integral. In this manner we obtain our final result for $\mathcal{S}'_B$ in $d = 1$ [218, 3, 4]:

$$\mathcal{S}'_B = i\frac{\theta}{4\pi} \int dx \int_0^{1/T} d\tau \mathbf{n} \cdot \left(\frac{\partial \mathbf{n}}{\partial x} \times \frac{\partial \mathbf{n}}{\partial \tau} \right) \tag{13.60}$$

where $\theta = 2\pi S$. Some comments and/or cautions about the derivation leading up to (13.60) are in order. The arbitrary way in which the sites in (13.59) were paired suggests that the answer is sensitive to the boundary conditions, and upon whether there are an even or odd number of sites in the system. There are indeed interesting boundary effects in the physics of antiferromagnetic spin chains [10, 11, 212], but we will not discuss them here. The overall sign of the answer in (13.60) also depends upon the sign of λ_i, but as we will see shortly, the physics is does not depend upon the sign of θ. Finally the result (13.60) can also be derived by analytic computations from (13.53): we can write the oscillating sum as half the spatial integral of the spatial derivative of the contribution of each site (by the same arguments leading to (13.59))– then using the fact that the triple product of $\partial\mathbf{n}/\partial x$, $\partial\mathbf{n}/\partial\tau$ and $\partial\mathbf{n}/\partial u$ must vanish we can obtain (13.60) using manipulations similar to those leading to (13.56).

In its present form, $\mathcal{S}'_B$ is the so-called topological θ-term, familiar in the particle theory literature. The co-efficient of θ in (13.60) computes a simple topological invariant which, for periodic boundary conditions in space, is always an integer. If we consider the field configuration $\mathbf{n}(x,\tau)$ as a map from two-dimensional spacetime, with periodic boundary conditions, to the surface of a unit sphere, then the topological invariant is simply the number of times spacetime has been wrapped around the

sphere. It is useful to visualize the simplest configuration of $\mathbf{n}(x,\tau)$ corresponding to the topological invariant of unity. Let the unit sphere be placed on an elastic sheet, representing space time. Now fold up the sheet to cover the sphere once: the orientation of $\mathbf{n}$ at (x,τ) is given by the point on the sphere adjacent to the point (x,τ) on the sheet. Such a spacetime configuration represents a tunneling event: deep in the past, or far in the future, $\mathbf{n}$ points to the north pole; however at some time, in a certain compact region of space, the $\mathbf{n}$ orientation tunnels all the way to the vicinity of the south pole and back; configurations with larger topologically invariants can be similarly interpreted. The result (13.23) implies that each such tunneling event yields a factor of $e^{i\theta} = (-1)^{2S}$ to the path integral for the partition function. This is the only consequence of the S'_B term. Of course, the terms in $\mathcal{S}_n$ give the usual positive weights (in imaginary time) also present for the rotor model. Notice that as θ is always an integral multiple of π, the sign of θ does not change the value of $e^{i\theta}$.

We are now able to state our principal conclusions, first reached by Haldane. For integer S, the phase factor with topologically non-trivial tunneling events is simply unity, and the theory reduces to the rotor model action $\mathcal{S}_n$, which has been studied in some detail in Chapters 5 and 6. On the other hand, for half-integer S, there are clearly substantial differences: the present formulation of the theory in (13.58) is however not a particularly convenient way of exploring the physics—it does tell us that the low energy properties of all the half-integer cases are the same, and we will explore the $S = 1/2$ case in the Chapter 14 by alternative methods.

We anticipate these results by sketching the renormalization group flows for the dimensionless coupling g for the cases $\theta = 0$ and $\theta = \pi$ in Fig 13.1. For the case of integer S, where $\theta = 0$, the flow just represents (6.8): all values of g flow eventually to strong coupling, and as we saw in Chapter 6, there is always an energy gap above the ground state. For the case $\theta = \pi$, the perturbative flow at small g is the same as before, as it is independent of θ. However, more sophisticated considerations [9, 5, 579, 152] to be discussed in Chapter 14, show that there is a fixed point at $g = g_c$, of order unity, which attracts all couplings with $g < g_c$. We will also see that the ground state is then a so-called 'Tomonaga-Luttinger liquid' and has gapless, linearly dispersing excitations. For $g > g_c$ (and $\theta = \pi$) the flow is again to strong coupling, and the ground state will be seen to be a 'spin-Peierls' state with an energy gap to all excitations (such a state will be described shortly below for $d = 2$).

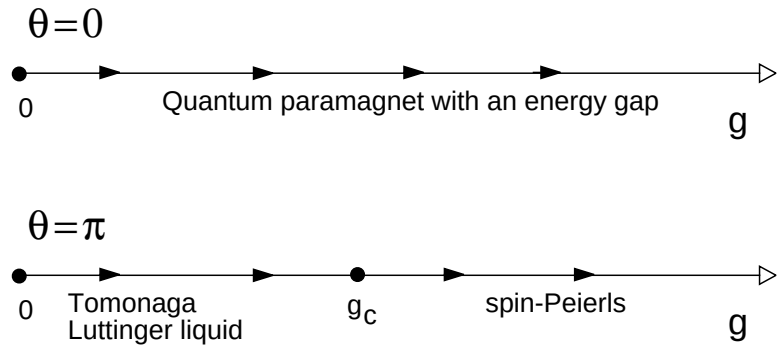

Fig. 13.1. Renormalization group flows for the dimensionless coupling g in (13.58) for $d = 1$ with $\mathcal{S}'_B$ given by (13.60). For $\theta = 0$, the flow is given by (6.8), and there is always an energy gap above the ground state. For $\theta = \pi$, there is a fixed point $g = g_c$, and near it the flow is $dg/d\ell \propto (g - g_c)^2$.

We conclude by reviewing a bit more explicitly the implications of the results of Chapters 5 and 6 for antiferromagnetic chains of integer spins. The mapping between correlation functions of the two theories is provided by (13.48). From this, we see that the correlator χ_u defined in (6.1) also specifies the fluctuations of the magnetization of the spin chain: at wavevector k this is a correlation function of the $\hat{\mathbf{S}}_i$ spins near the wavevector $q = k$. Further the correlations of the order parameter $\mathbf{n}$ given by χ in (5.2) at wavevector k, map onto correlations of $\hat{\mathbf{S}}_i$ at wavevector $q = k + Q$, where $Q = \pi/a$ is the ordering wavevector of the classical antiferromagnetic chain; all of the results for the rotor correlation functions in Chapter 6 can therefore be applied to integer spin antiferromagnets. We saw in Chapter 6 that the $d = 1$, $N = 3$ quantum rotor model always had a gap: the same is therefore true of integer spin antiferromagnetic chains–this is the so-called Haldane gap (we will see in the following chapter that half-integer spin chains can be gapless). The $T = 0$ spectrum of the integer spin antiferromagnets is qualitatively the same as that discussed in the strong coupling expansion in Section 5.1.1: the lowest excited states are a triplet of $S = 1$ particles with infinite lifetime: for the spin chain, this particle appears as a pole in the $\hat{\mathbf{S}}$-$\hat{\mathbf{S}}$ correlation function which has its minimum at $q = \pi/a$. Higher excited states consist of multi-particle continua of this triplet of particles.

13.3.1.2 $d = 2$

We will consider the properties of the theory (13.58) on the $d = 2$ square lattice.

This requires evaluation of the oscillating sum in $\mathcal{S}'_{\mathcal{B}}$ in (13.53). Using techniques very similar to those used in $d = 1$, it is not difficult to establish an important result: $\mathcal{S}'_B$ vanishes for all smooth spacetime configurations of $\mathbf{n}(x, \tau)$. Simply evaluate (13.53) row by row on the square lattice. The sum on each row is precisely the same as that carried out in $d = 1$, and equals (13.60) on each row, up to an overall sign. Moreover, because of the structure of the sublattices, this overall sign will oscillate as we move from row to row. Now, note that the arguments in Section 13.3.1.1 imply that the contribution of each row is quantized in integer multiples of θ. If, as we are assuming, $\mathbf{n}(x, \tau)$ is smoothly varying, the contribution of the rows must also change smoothly as we move from row to row. This is only compatible with the quantization if each row yields precisely the same integer. Hence their oscillating sum appearing in $\mathcal{S}'_B$ vanishes.

However, this is not the end of the story. It turns out there are important *singular* configurations of $\mathbf{n}(x, \tau)$ that do yield a non-vanishing contribution to $\mathcal{S}'_B$. We postpone discussion of the consequences of these contributions until later in this subsection; first, we discuss the implication of the results of Part 2 for square lattice antiferromagnets, assuming that $\mathcal{S}'_B$ vanishes identically for all S.

The properties of the $N = 3$, $d = 2$ quantum rotor model were first discussed using the large N expansion in Chapter 5), and then in some more detail in Chapters 7, 8, and 9. The most significant feature of these results was the existence of a quantum phase transition at a critical value $g = g_c$, separating a magnetically ordered ground state from a quantum paramagnetic ground state.

The magnetically ordered state of the rotor model corresponds to a "Néel" ground state of the antiferromagnet: this is a state in which the spin-rotation invariance of the Hamiltonian (13.1) is broken because of a non-zero, expectation value of the spin operator, which takes opposite signs on the two sublattices: from (13.48) we see

$$\left\langle \hat{\mathbf{S}}_i \right\rangle \propto \lambda_i S \left\langle \mathbf{n}(x_i) \right\rangle = S N_0 \mathbf{e}_z, \tag{13.61}$$

where $\mathbf{e}_z$ is a unit vector pointing the $\mathbf{e}_z$ direction (say) of spin space. Note that there was no state with such a broken symmetry in $d = 1$. The missing proportionality constant in (13.61) depends upon microscopic

details, and is not of any importance: in Part 2 we expressed physical properties of the rotor model on the ordered side in terms of N_0: these can be applied unchanged to the antiferromagnet simply by replacing N_0 by the actual expectation value of $\lambda_i \left\langle \hat{\mathbf{S}}_i \right\rangle$. As in $d = 1$, correlators of $\mathbf{L}$ at wavevector $\vec{k}$ map onto correlators of $\hat{\mathbf{S}}$ at $\vec{q} = \vec{k}$, while correlators of $\mathbf{n}$ at $\vec{k}$ map onto $\vec{q} = \vec{k} + \vec{Q}$, with $\vec{Q} = (\pi/a, \pi/a)$ the ordering wavevector. As was the case for the rotor model, the broken rotational invariance is restored at any non-zero temperature, and the antiferromagnet instead acquires an exponentially large correlation length given by (7.10) and (7.20). In these results, we take for the value of ρ_s the actual $T = 0$ spin stiffness of the quantum antiferromagnet. The non-zero temperature static and dynamic correlations are described by (7.1), with the function Φ_- as described in Chapter 7.

Numerical studies of the square lattice antiferromagnets with nearest neighbor antiferromagnets have shown fairly conclusively that the ground state has Néel order for all values of S including $S = 1/2$ [431, 253]. Thus it appears that all such antiferromagnets map onto the rotor model with $g < g_c$. For $S = 1/2$ it has been argued [102, 103] that the value of g is sufficiently close to g_c so that the universal crossover between the low and high T limits of the continuum rotor field theory shown in Fig 5.2 can be observed with increasing temperature, as we have discussed in Section 5.5. For larger S, the antiferromagnets appear to go directly from the universal low T region on the ordered side of Fig 5.2 to a non-universal lattice high T region [144].

Clearly, it would also be physically interesting to find collinear antiferromagnets which map onto rotor models with $g > g_c$, and therefore do not have Néel order in their ground state. A convenient choice, studied extensively in the literature, has been the square lattice antiferromagnet with first and second neighbor antiferromagnetic exchanges, labeled J_1 and J_2 respectively. The classical limit of this model has collinear Néel order for all J_2/J_1, and so the quantum fluctuations should continue to be described by (13.58). Numerical and series expansion studies [91, 97, 119, 158, 186, 185, 375, 413, 480, 481, 329] for $S = 1/2$ have shown that this model loses the order (13.61) around $J_2/J_1 = J_c \approx 0.4$. So we can identify the point $J_2/J_1 = J_c$ with the quantum critical point $g = g_c$ of the rotor model. The quantum paramagnetic state of the rotor model should therefore yield the characteristics of the antiferromagnet with J_2/J_1 just above J_c: spin rotation invariance is restored, and there

is a gap to all excitations. Nonzero temperature properties are described by (7.3) with Δ_+ the actual energy gap of the antiferromagnet.

One important property of the quantum paramagnetic state of the rotor model deserves special mention, as it has crucial implications for the corresponding antiferromagnet. Recall that the excited states of the rotor model were described in terms of a N-fold degenerate quasiparticle and its multiparticle continua. This lead to the spectrum shown in Fig 4.1 and discussed in the strong-coupling expansion of Section 5.1.1: there is an infinitely sharp delta function in $\mathrm{Im}\chi(k,\omega)$ at the position of the quasi-particle energy $\omega = \varepsilon_k$. For $N = 3$, this is clearly a quasiparticle with total angular momentum $S = 1$; so the dominant excitation of this phase of quantum antiferromagnet is a $S = 1$ particle with its energy minimum at $\vec{q} = \vec{Q}$, and this will lead to a delta function in the dynamic spin susceptibility at wavevectors near $\vec{Q}$. Note that this $S = 1$ particle exists for all values of the spin S of the individual spins of the underlying antiferromagnet. This gapped $S = 1$ excitation should also be contrasted with the spin-wave excitations of the ordered Néel state which are gapless, two-fold degenerate, and do not carry definite total spin (although they are eigenstates of total $\hat{S}_z$, with eigenvalues ± 1 for a Néel state polarized in the z direction).

We conclude this subsection by returning to consideration of $\mathcal{S}'_B$, the consequences of which have been ignored so far. A full computation is quite technical and lengthy, and we will be satisfied here by highlighting some essential features, and refer the reader to the original literature for further details [426, 427]. Before outlining the calculation, let us describe the consequences of $\mathcal{S}'_B$ in simple physical terms. There are two important results that emerge:

(*i*) All of the results above on the nature of the quantum critical point, and on the crossovers in its vicinity on both the Néel ordered and quantum paramagnetic side remain unchanged [381, 469, 103].

(*ii*) On certain lattices, and for certain values of S, a new spontaneously broken lattice symmetry emerges everywhere in the quantum paramagnet [426] (spin rotation invariance remains unbroken in the quantum paramagnet, and there is no change in the structure of the Néel state). This broken symmetry is associated with the appearance of *spin-Peierls* order, which we will describe momentarily.

It is believed that the spin-Peierls order parameter does not play an essential role in the quantum critical point noted in (*i*), and that its fluctuations only become important at sufficiently low energies and long distances so as not to modify the crossovers of the quantum rotor model

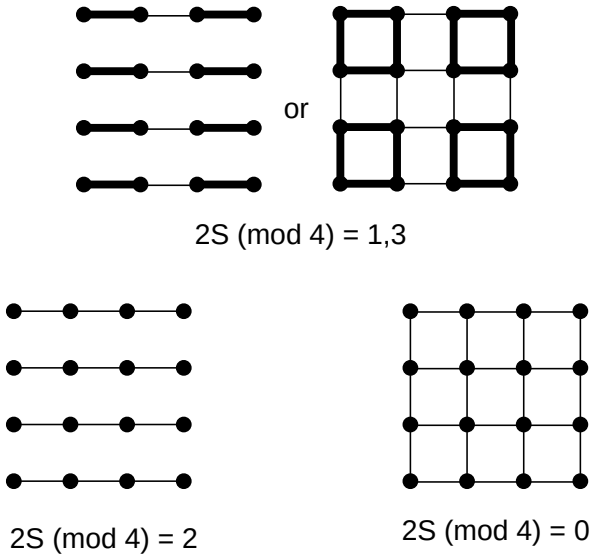

Fig. 13.2. Quantum paramagnetic ground states of the weakly frustrated square lattice antiferromagnet as a function of $2S(\text{mod } 4)$. The values of P_{ij} on the nearest neighbor links are schematically indicated by the different kinds of lines on the links; those on thick lines are larger than those on the thin lines, and weakest are on the empty links.

computed in Part 2. To describe the spin-Peierls order, consider the quantity

$$P_{ij} = \left\langle \hat{\mathbf{S}}_i \cdot \hat{\mathbf{S}}_j \right\rangle . \tag{13.62}$$

Note that P_{ij} is a scalar under spin rotations, and so a non-zero value does not break a spin rotation symmetry. The Hamiltonian H_S in (13.1) is also invariant under a group of lattice symmetries (involving lattice rotation, reflection and translations), and the values of the P_{ij} for all pairs sites i, j should, in general, also respect these symmetries. A spin-Peierls state is one in which the values of P_{ij} break a lattice symmetry; this broken symmetry will be observable experimentally in lattice distortions whose pattern will reflect that in P_{ij}—the distortion arise from the coupling between the spin exchange energy and phonon displacements which have not been included in the Hamiltonians we are considering here. For the case of a square lattice with first and second neighbor interactions, the quantum paramagnet with J_2/J_1 just above J_c possesses spin-Peierls order of the type shown in Fig 13.2. For $S = 1/2$, like values

of P_{ij} line up in columns or plaquettes which clearly break symmetry of rotation by 90 degrees about each lattice point; the ground state is four-fold degenerate, and a similar spin-Peierls ordering is expected for all half-integral S. If it was possible to obtain a quantum paramagnet for $S = 1$ (or other odd integer S) by a continuous transition from a Néel state, then it is predicted to have a two-fold degenerate ground state, with the P_{ij} on the horizontal bonds differing from those on the vertical bonds (see Fig 13.2). Finally, only for even integer S, is the paramagnetic state non-degenerate and breaks no lattice symmetry [10, 11]. Related results exist for quantum paramagnetic states accessed by a continuous transition from other collinear states on the square or other lattices. In all cases there are special values of S for which the quantum paramagnet is non-degenerate and has no spin-Peierls order; these special values extend to all values of S only for lattices with small symmetry groups.

Let us , finally, consider the complete evaluation of $\mathcal{S}'_B$, and discuss its relationship to the spin-Peierls ordering just described. We will consider the case of the square lattice with nearest neighbor exchanges, and possible further neighbor exchanges which do not destroy the collinear, two sublattice ordering of the classical Néel state. We have already argued at the beginning of this subsection that $\mathcal{S}'_B$ vanishes for smooth spacetime configurations of $\mathbf{n}(x, \tau)$. We should therefore consider singular configurations, and for the case of 3-component vector order parameter, the only topologically stable possibility is the so-called 'hedgehog' singularity [219]. This is a singularity occurring at point in spacetime and corresponds to a tunneling event in which the 'Skyrmion number', Y, of a given time slice of $\mathbf{n}(x, t)$ changes. The latter is defined by the spatial integral

$$Y(\tau) = \frac{1}{4\pi} \int d^2x \mathbf{n} \cdot \left(\frac{\partial \mathbf{n}}{\partial x_1} \times \frac{\partial \mathbf{n}}{\partial x_2} \right). \tag{13.63}$$

Compare (13.63) to the topological θ term in $d = 1$ of (13.60): the two expressions are identical except that we now have an integral over space only, while earlier we had a spacetime integral. By the same arguments as made below (13.60), Y is an integer for periodic boundary conditions in space. Let us describe a hedgehog tunneling event in which Y changes from 1 to 0, in a pictorial language used by Haldane [219]. As below (13.60) we can represent a configuration with $Y = 1$ as an elastic sheet (now representing space, rather than spacetime) wrapped on a sphere. In reality, the spins lie on a lattice, and so the elastic sheet has a fine square mesh on it. Now imagine a tunneling event in which

one square on the mesh expands and allows the sphere to pass through; the resulting configuration will have its Y changed to 0. It remains to evaluate the summation in (13.53) for the evolution of $\mathbf{n}(x,\tau)$ just described. Actually, we cannot consider hedgehog tunneling events singly, as then the periodic boundary conditions in τ, required for a meaningful evaluation of (13.53), will not be satisfied. We therefore consider a sequence of events at well separated times, centered at the midpoints of plaquettes labeled a, and involving the change in Skyrmion number ΔY_a such that $\sum_a \Delta Y_a = 0$. These events are to be considered as saddle points in the evaluation of the coherent state path integral of the lattice antiferromagnet: the configuration of $\mathbf{n}(x,\tau)$ at the saddle point minimizes the action, and, provided the hedgehogs are well separated, can reasonably be expected to have four-fold rotational symmetry about the plaquette a around which the tunneling occurs. As at the beginning of Section 13.3.1.1, let us write $\mathcal{S}'_B$ as

$$\mathcal{S}'_B = S\sum_i \lambda_i \mathcal{A}_i, \tag{13.64}$$

where $\mathcal{A}_i$ is the contribution of site i. Now we can evaluate $\mathcal{A}_i$ by following the area swept out on the unit sphere by each site on the elastic sheet during the tunneling event: from this it is simple to see the following important intermediate result—the lattice configuration of $\mathcal{A}_i$ has a vortex of strength $4\pi\Delta Y_a$ around plaquette a. As the sum in (13.64) cannot change from smooth changes in the lattice configuration of $\mathcal{A}_i$, we need only take a representative configuration which has the proper vortex singularities; for instance, we can take

$$\mathcal{A}_i = 2\sum_a \Delta Y_a \arctan\left(\frac{x_{i1}-X_{a1}}{x_{i2}-X_{a2}}\right), \tag{13.65}$$

where $x_{i1,2}$ are the components of the lattice points x_i, and X_a is the position of the center of plaquette a. We have to insert (13.65) into (13.64) and evaluate the sum over i. This is a mathematical step, and the details are given by Haldane [219]: it is not difficult to see that the result takes the form

$$\mathcal{S}'_B = i\pi S\sum_a \Delta Y_a \zeta_a. \tag{13.66}$$

The values of the ζ_a depend upon the co-ordinates of plaquette a; a number of choices for these values are possible, but $e^{-\mathcal{S}'_B}$ remains the same provided $\sum_a \Delta Y_a = 0$. A particular choice is $\zeta_a = 0,1,2,3$ if the co-ordinates X_a are (even,even), (even,odd), (odd,odd), (odd,even).

Now a last step remains: we have to sum over all possible hedgehog events, while including the phase factors arising from $e^{\mathcal{S}'_B}$ with each such event. Refs [426, 427] showed how such a summation could be carried out systematically in a certain large N expansion: describing this here would take us too far afield, and we refer the reader to Ref [427] for fairly explicit details. The hedgehog events are completely suppressed by the action arising from $\mathcal{S}_n$ for $g < g_c$, and therefore have no significant consequence for the Néel phase. In contrast, for $g > g_c$, these events proliferate, and it was shown in the quoted papers how the Berry phases in (13.66) necessarily led to a spontaneously broken symmetry and the appearance of the spin-Peierls order that has already been described. Note that for S even integer, (13.66) is always an integral multiple of $2\pi i$, and so $\mathcal{S}_B$ has no effect—the properties in this case are therefore the same as the rotor model, and there is no spin-Peierls order [10].

The reader may object that the above arguments for the ubiquity of spin-Peierls order in collinear $S = 1/2$ antiferromagnets rely on theories obtained in a semiclassical large S limit, and could possibly break down at small S. This issue has been addressed by studies designed to directly study $S = 1/2$ quantum antiferromagnets either by phenomenological [299, 436] or large N approaches [425]. Neighboring spins are assumed to form singlet bonds in pairs, and then the low-lying, spin-singlet excitations arise from resonance between different arrangements of the bonds (the 'resonating valence bond' picture [22, 42]). From both approaches, the so-called *quantum dimer model* [436] appears as an effective Hamiltonian for the low energy spin-singlet states. This latter model can be studied quite reliably by a series of duality transformations [582, 427, 175, 463] and an 'instanton' gas model emerges which is, quite remarkably, *equivalent* to the hedgehog gas model obtained above from a semiclassical perspective. In particular, each instanton has a Berry phase which is given precisely by (13.66). In this context, the phases in (13.66) are a consequence of the constraint that each $S = 1/2$ spin can form a valence bond with exactly one of its neighbors, whereas, here we obtained (13.66) from a very different coherent state path integral. The identity of these two distinct approaches reinforces our confidence in the correctness of (13.66), and to the presence of spin-Peierls order for $S = 1/2$, which follows quite robustly [427] from it. The quantum dimer model has also been examined in exact diagonalization studies, and again the evidence for spin-Peierls order is quite convincing [330].

13.3.2 Non-collinear ordering and deconfined spinons

We turn to consideration of quantum antiferromagnets which have more complicated ordered magnetic states than those described so far. We will consider models (13.1) on non-bipartite lattices, or with further neighbor interactions so that simple collinear states are not likely to be the ground states. Throughout, we will only be considering states which do not have a macroscopic magnetic moment, *i.e.,* the expectation value of $\sum_i \hat{\mathbf{S}}_i$ in any low-lying state is not of the order of the number of sites in the system. Such states are expected to be preferred in models with all $J_{ij} < 0$. Also we will only consider the case of $d = 2$ here, as $d = 1$ antiferromagnets are better treated by the methods of the following chapter.

The simplest, and most thoroughly studied example of a non-collinear antiferromagnet is the triangular lattice with a nearest-neighbor antiferromagnetic exchange. In the limit $S \to \infty$, the classical ground state is easy to work out: it is characterized by the expectation value

$$\left\langle \hat{\mathbf{S}}_i \right\rangle = S \left(\mathbf{n}_1 \cos(\vec{Q} \cdot \vec{x}_i) + \mathbf{n}_2 \sin(\vec{Q} \cdot \vec{x}_i) \right), \tag{13.67}$$

where the ordering wavevector $\vec{Q} = (4\pi/a)(1/3, 1/\sqrt{3})$ on a triangular lattice with $(a, 0, 0)$ one of the vectors connecting nearest-neighbor lattice sites, and $\mathbf{n}_{1,2}$ are arbitrary vectors in spin space satisfying

$$\mathbf{n}_1^2 = \mathbf{n}_2^2 = 1 \quad ; \quad \mathbf{n}_1 \cdot \mathbf{n}_2 = 0 \tag{13.68}$$

These constraints define two orthogonal unit vectors, and each such pair defines a different classical ground state. This is a key difference from the collinear states in Section 13.3.1.2, where only a *single* unit vector was sufficient to characterize the ground state, as in (13.61). Alternatively stated, the order parameter characterizing the broken symmetry in the classical ground state is a *pair* of orthogonal vectors [222, 136]. One possible ground state is shown in Fig 13.3, for the case where $\mathbf{n}_1$, $\mathbf{n}_2$ lie in the plane of the lattice. Other antiferromagnets with *coplanar* ordering in their classical ground states can be treated in an essentially identical manner. Another important example studied in the literature is the square lattice antiferromagnet with first, second, and third neighbor exchanges (the J_1-J_2-J_3 model). For a range of parameters this model has an incommensurate spiral ground state: such an ordering is described as in (13.67), but the wavevector $\vec{Q}$ is no longer pinned at a precise value, and varies continuously as the values of exchange constants are changed. As we move from site to site in the direction $\vec{Q}$ the

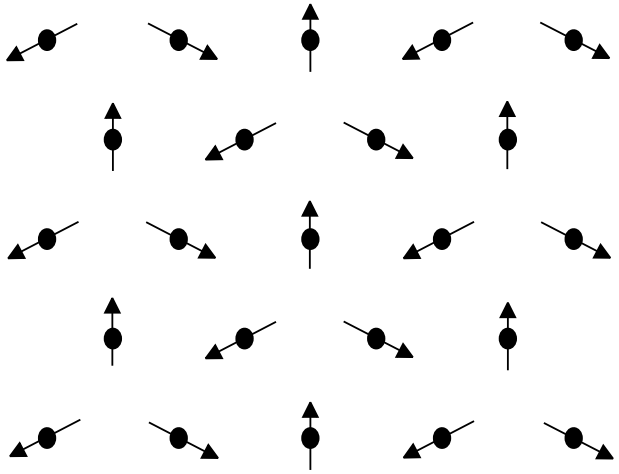

Fig. 13.3. Magnetically ordered ground state on the triangular lattice. The spins have been taken to lie in the plane of the triangular lattice, but this need not generally be the case.

spin orientation rotates by some irrational angle in the plane defined by $\mathbf{n}_1$ and $\mathbf{n}_2$. Finally antiferromagnets in which the spin arrangement is not even coplanar but genuinely three-dimensional can be treated using similar methods, but will not be considered here.

Instead of working with vectors $\mathbf{n}_1$, $\mathbf{n}_2$ which satisfy the constraints (13.68), it is convenient to introduce an alternative parameterization of the space of ground states. It takes 6 real numbers to specify the two vectors $\mathbf{n}_1$, $\mathbf{n}_2$, and the 3 constraints (13.68) reduce the degrees of freedom to 3. We can use these 3 real numbers to introduce two complex numbers z_1, z_2 subject to the single constraint

$$|z_1|^2 + |z_2|^2 = 1. \tag{13.69}$$

We relate these numbers to $\mathbf{n}_1$, $\mathbf{n}_2$ by [25, 104]

$$n_{2\alpha} + i n_{1\alpha} = \sum_{a,b,c=1}^{2} \varepsilon_{ac} z_c \sigma^{\alpha}_{ab} z_b, \tag{13.70}$$

where $\alpha = x, y, z$, σ^{α} are the Pauli matrices, and ε_{ab} is the second-rank antisymmetric tensor $\varepsilon_{12} = -\varepsilon_{21} = 1$, $\varepsilon_{11} = \varepsilon_{22} = 0$. The reader can check that the parameterization (13.70) for $\mathbf{n}_{1,2}$ automatically satisfies (13.68) provided the single constraint (13.69) holds. So we have succeeded in reducing the number of constraints down from 3 to 1. However the mapping from $z_{1,2}$ to $\mathbf{n}_{1,2}$ is not one-to-one but two-to-one; the

two-fold redundancy is apparent from (13.70) as z_a and $-z_a$ correspond to precisely the same $\mathbf{n}_{1,2}$, and therefore the same spin configuration; this redundancy will be crucial to our subsequent considerations. To describe it further, let us decompose z_a into its real and imaginary parts

$$z_1 = m_1 + im_2 \quad ; \quad z_2 = m_3 + im_4. \tag{13.71}$$

Then the order parameter becomes a 4-component, real vector m_ρ ($\rho = 1, 2, 3, 4$) and (13.69) translates into the constraint that this vector has unit length (of course, there is no reason the effective action for m_ρ should be invariant under O(4) rotations in this space–the underlying symmetry is always O(3)). The identity of z_a and $-z_a$ means that m_ρ is a *headless* vector, much like a nematic liquid crystal, which is described by a headless 3-vector.

We can proceed to examine the quantum fluctuations about the above classical states by precisely the same strategy as that followed in Section 13.3.1.2. We allow $\mathbf{n}_{1,2}$, and therefore z_a, to be slowly varying functions of spacetime. We also introduce a slowly varying uniform magnetization field $\mathbf{L}(x,t)$ such that the spatial integral over $\mathbf{L}$ is precisely the total magnetization. Then, following (13.48) we parameterize

$$\begin{aligned}\mathbf{N}(i,\tau) = \Big(\mathbf{n}_1(x_i,\tau)\cos(\vec{Q}\cdot\vec{x}_i) + \mathbf{n}_2(x_i,\tau)\sin(\vec{Q}\cdot\vec{x}_i)\Big) \\ \times\sqrt{1 - v^2\mathbf{L}^2(x_i,\tau)} + v\mathbf{L}(x_i,\tau),\end{aligned} \tag{13.72}$$

where v is the volume per site. This is to be inserted in the coherent state path integral of H_S in (13.1) and the result expanded in gradients. Finally the uniform magnetization variable $\mathbf{L}$ is to be integrated out as below (13.56). The steps are similar to those in Section 13.3.1.2 and will not be explicitly carried out. Rather, let us try to anticipate the form of the answer on general symmetry grounds.

We list the constraints that must be obeyed by the final effective action:
(i) We must clearly require invariance under spin rotations. These are realized by the global $SU(2)$ transformation

$$\begin{pmatrix} z_1 \\ z_2 \end{pmatrix} \to U \begin{pmatrix} z_1 \\ z_2 \end{pmatrix} \equiv \begin{pmatrix} \alpha & \beta \\ -\beta^* & \alpha^* \end{pmatrix} \begin{pmatrix} z_1 \\ z_2 \end{pmatrix} \tag{13.73}$$

where α and β are complex numbers satisfying $|\alpha|^2 + |\beta|^2 = 1$. Applying this to (13.70), we see that this performs the rotation $n_{1,2\alpha} \to R_{\alpha\beta} n_{1,2\beta}$ where

$$U^\dagger \sigma^\alpha U = R_{\alpha\beta}\sigma^\beta \tag{13.74}$$

(*ii*) Next, we consider the consequences of lattice translations. Any spatial configuration of $\mathbf{n}_{1,2}(x,\tau)$ should have its energy unchanged under translation by a lattice vector $\vec{y}$. By combining (13.70) with (13.72) we see that such a translation is realized by a simple overall phase change of the z:

$$z_a \to e^{-i\vec{Q}\cdot\vec{y}/2} z_a. \tag{13.75}$$

Note that this transformation is not a special case of (13.73), which was restricted to unitary matrices with unit determinant. For the case of the triangular lattices (13.75) requires that the action be invariant under multiplication of z_a by the cube roots of unity. For incommensurate spiral states, by different choices of $\vec{y}$ we see that (13.75) requires invariance under multiplication of z_a by an arbitrary U(1) phase factor.
(*iii*) Finally, let us recall the two-fold redundancy in the mapping from z_a to the $\mathbf{n}_{1,2}$ discussed below (13.70). The change in sign of z_a can vary from point to point in spacetime with no consequence for the $\mathbf{n}_{1,2}$: therefore, we require invariance under the discrete Z_2 gauge transformation

$$z(x,\tau) \to \eta(x,\tau) z(x,\tau) \tag{13.76}$$

where $\eta(x,\tau) = \pm 1$ but can otherwise vary arbitrarily. In the naive continuum limit, the gauge nature of the transformation (13.76) does not impose any additional constraints beyond those arising from a constant η. However, the theory has to be regularized at short scales, and the Z_2 gauge symmetry does impose additional constraints on any effective lattice action. Moreover, the invariance (13.76) will also play a crucial role in the nature of the possible topological defects.

Let us write down the simplest action consistent with the above constraints in the naive continuum limit. Up to second order in spatial gradients, there are only two independent terms: $|\nabla z_a|^2$ and $|z_a^* \nabla z_a|^2$ (a third possibility, $|\varepsilon_{ab} z_a \nabla z_b|^2$ satisfies a simple linear relation with these two). Identical considerations also apply to the terms with two temporal gradients. We are therefore led to the following effective action for the z_a, which plays the role of $\mathcal{S}_n$ in Section 13.3.1.2

$$\mathcal{S}_z = \int d^2x d\tau \sum_{\mu=\vec{x},\tau} \frac{1}{g_\mu} \left[|\partial_\mu z_a|^2 + \gamma_\mu |z_a^* \nabla z_a|^2 \right] \tag{13.77}$$

where g_x, g_τ, γ_x and γ_τ are coupling constants. In addition, as in Section 13.3.1.2, there could be Berry phases, associated with singular

configurations of the z_a. These have to be analyzed on a lattice-by-lattice basis and are not completely understood.

However, even at the level of the action $\mathcal{S}_z$, and ignoring possible Berry phases, open questions remain (in contrast, the action $\mathcal{S}_n$ is believed to be quite thoroughly understood). There are vexing differences among different ways of analyzing $\mathcal{S}_z$: numerical simulations and renormalization group analyses using expansions in $(d-1)$, $(3-d)$, or the inverse of the number of z_a components [130, 26]. There is little doubt that the fate of the Z_2 gauge symmetry (13.76) plays a crucial role in these differences, as the different approaches treat it in quite inequivalent manners. In particular, the system allows a Z_2 vortex excitation, and the nature of the quantum paramagnet depends upon whether such vortices proliferate or are suppressed. Because of the importance this vortex, let us describe its structure more carefully. The vortex is best visualized in terms of the headless vector m_ρ: as one circles the core of the vortex, m_ρ rotates by 180 degrees about a fixed axis orthogonal to m_ρ. So upon returning to the original point, m_ρ has now turned into $-m_\rho$, but this is acceptable as the overall sign of m_ρ is not significant (in mathematical terms, the order parameter m_ρ belongs to the space S_4/Z_2, and the vortex is associated with its first homotopy group Z_2). An especially clear discussion of such vortices, and their relationship to the Z_2 gauge symmetry has been given by Lammert *et al.* [314] in the context of nematic liquid crystals, and the reader is urged to consult their paper. In the present quantum problem, there could also be important Berry phases associated with the Z_2 vortices, with values depending upon microscopic details, as was found for the hedgehogs in Section 13.3.1.2.

We will not survey all earlier approaches to the analysis of $\mathcal{S}_z$ here, but highlight a promising scenario which has some striking consequences for the quantum paramagnet. This scenario emerged first in a direct large N study [428, 464, 444] of the quantum antiferromagnet (13.1) on frustrated lattices, and related results emerge from studies of the continuum theory $\mathcal{S}_z$ in an expansion in the inverse of the number of z_a components, or in an expansion in $(d-1)$ [33, 104, 34, 107]. There are two phases: a magnetically ordered phase and a quantum paramagnet, and these are separated by a second order quantum phase transition. The Z_2 vortices are obviously suppressed in the magnetically ordered phase by the non-zero spin stiffness, but they remain suppressed in the quantum paramagnet, as is also found to be the case in the corresponding phases of the nematic liquid crystal [314]. The physical properties of

both phases can be rapidly understood by considering the case $\gamma_\mu = 0$ in (13.77), although this special value will not modify the general form of the following results. For $\gamma_\mu = 0$, we insert (13.71) into (13.77), and see straightforwardly that the action $\mathcal{S}_z$ is symmetric under O(4) rotations of the m_ρ, and becomes precisely equivalent to the $N = 4$ case of the quantum rotor model $\mathcal{S}_n$ studied intensively in Part 2. The properties of $\mathcal{S}_z$ therefore follow directly from the results of Part 2. The magnetically ordered phase has $3 = 4-1$ linearly dispersing spin wave excitations, and magnetic order disappears at any non-zero temperature. The quantum paramagnetic phase has an energy gap, Δ_+, and the excitations are built out of the Fock space of a 4-fold degenerate particle.

Despite the mapping above to Part 2, there is a crucial distinction in the physical interpretation of the structure of the quantum paramagnet. Its particle excitations are the bosonic quanta of the z_a field, and the transformation (13.73) under spin rotations makes it clear that these bosons carry spin $S = 1/2$. (This accounts for a 2-fold degeneracy of the particle states; an additional factor of 2 comes from accounting for the particle and anti-particle states). This should be contrasted with the $S = 1$ particle that was found in the quantum paramagnetic with collinear correlations in Section 13.3.1.2. These $S = 1/2$ bosonic particles are labeled 'spinons': we can view the $S = 1$ particle as the bound state of two $S = 1/2$ particles, and therefore a quantum transition from a quantum paramagnet with collinear correlations to one with non-collinear correlations can be viewed as one of the deconfinement of spinons: a simple theory for such a transition has been discussed in Refs [428, 464, 444]. Here let us discuss an important physical property of a quantum paramagnet with deconfined spinons: we compute the dynamic susceptibility at the non-collinear ordering wavevector, defined by

$$\chi(k, i\omega_n)\delta_{\alpha\beta} = \frac{v}{M}\sum_{i,j}\int_0^{1/T} d\tau \left\langle \hat{S}_{i\alpha}(i\tau)\hat{S}_{j\beta}(0)\right\rangle e^{-i((\vec{k}+\vec{Q})\cdot(\vec{x}_i-\vec{x}_j)-\omega_n\tau)}. \tag{13.78}$$

Using (13.70) and (13.72) we see that (ignoring the contribution of $\mathbf{L}$, which will only renormalize a pre-factor that can absorbed into a redefinition of the quasiparticle amplitude $\mathcal{A}$):

$$\chi(k, i\omega_n) = \frac{S^2}{6}\sum_{a,b=1}^{2}\int d^2x \int_0^{1/T} \langle z_a(x, i\tau)z_b(x, i\tau)z_a^*(0, 0)z_b^*(0, 0)\rangle . \tag{13.79}$$

So χ is given by the propagator of *two spinons*, rather than the single particle propagator which appeared in (5.2). As discussed above, the z quanta of the quantum paramagnet have a quasiparticle pole at $T = 0$ as in (4.99) or (5.30); the contribution of this pole leads to the expression

$$\chi(k, \omega_n) = \mathcal{A}^2 S^2 \Pi(k, \omega_n), \tag{13.80}$$

where the two-particle propagator Π was discussed in (7.42). At $T = 0$, taking the imaginary part of (7.46) we obtain

$$\mathrm{Im}\chi(k, \omega) = \frac{\mathcal{A}^2 S^2}{8c^2} \frac{\mathrm{sgn}(\omega)}{\sqrt{\omega^2 - c^2 k^2}} \theta \left(|\omega| - (c^2 k^2 + 4\Delta_+^2)^{1/2} \right), \tag{13.81}$$

where θ is the unit step function. So there is no pole in $\chi(k, \omega)$ as there was for the case of a quantum paramagnet with collinear spin correlations; rather there is a branch cut at frequencies greater than $(c^2 k^2 + 4\Delta_+^2)^{1/2}$, which corresponds to the threshold for the creation of a *pair* of spinons. This branch cut is a characteristic property of the deconfinement of spinons in a quantum paramagnet.

We emphasize that the suppression of the Z_2 vortices was crucial to the existence of the free bosonic spinons in this quantum paramagnet. In the absence of such vortices, it is possible to consistently assign a global phase to a spinon wavefunction without any sign ambiguities. The wavefunction of a spinon changes in sign upon transport around a Z_2 vortex, and so spinons are expected to confine into integer spin excitations when such vortices proliferate [428, 464].

We close this subsection by noting some related issues that have been discussed in the literature.

A spinon-based approach can also be used to describe the collinear antiferromagnets of Section 13.3.1. One obtains the action (13.77), but at the special point $\gamma_\mu = 1$, where the reader can easily check that it is invariant under the $U(1)$ gauge transformation $z_a(x, \tau) \to e^{i\eta(x,\tau)} z_a(x, \tau)$. This theory has been analyzed by a number of methods [564, 118, 426, 427, 72, 106] with the conclusion that the spinons are *confined*, and the resulting spectrum is in agreement with the form already obtained in Section 13.3.1 by other methods.

Another possible quantum paramagnetic state of frustrated antiferromagnets is the "chiral spin liquid" [282, 317, 561, 223] (and the related 'flux phase' [13]). In this state, the local spin correlations are not only non-collinear, but also non-coplanar, and the ground state breaks parity and time-reversal invariance. Classically, it is quite difficult to construct antiferromagnets with non-coplanar spin ordering in the ground

states: some rather intricate lattices or multiple spin couplings are usually necessary. The chiral spin liquid would then be accessed by quantum disordering transition from such a magnetically ordered state. The interest in such a state has been driven primarily by the fact its excitations have rather remarkable properties: they are $S = 1/2$ spinons which obey fractional statistics. Furthermore, it has been predicted that doping such a state would lead to a new type of 'anyonic' superconductivity [316, 317, 156, 226, 93]. However, no experimental realization of this exotic possibility has so far been found. There have also been arguments [317] that $S = 1/2$ spinon excitations of any two dimensional quantum paramagnet should obey fractional statistics; this appears to be in disagreement [464] with the bosonic spinon states discussed in the body of this section.

13.4 Partial polarization and canted states

This section will interpolate between the ferromagnetic states studied in Section 13.2, with maximum uniform spin polarization in their ground states, and the antiferromagnets of Section 13.3, which had a thermodynamically negligible spin polarization. One way to do this would be examine the ground states of models H_S in (13.1) at $\mathbf{H} = 0$, but with a set of J_{ij} which can take both signs. Models of this type were examined in Ref [466], and it was argued that they could be described by a ferromagnetic extension of the rotor models studied in Part 2. The properties of such models are quite intricate, and we refer the reader to the original paper for further details. Here, we shall look at a closely related model whose properties are significantly simpler to delineate. We will begin with an antiferromagnet with all $J_{ij} < 0$, and attempt to force in a macroscopic moment by placing it in a strong uniform field $\mathbf{H}$. So the uniform magnetization will not arise spontaneously from ferromagnetic exchange interactions, but will instead be induced by an external field. This will cause important differences in nature of certain spin-wave excitations, which are no longer required to be gapless due to the explicit breaking of rotational invariance in the Hamiltonian. Nevertheless, numerous other features will be very similar to the far more complicated models considered in Ref [466]. Further, the case of an antiferromagnet in a strong uniform field is of direct physical importance, having been investigated in several recent experiments, as we shall discuss in Section 13.5.

The low energy properties of an antiferromagnet in a field $\mathbf{H}$ are de-

scribed by the action $\mathcal{S}_n$ in (13.58) or (5.16). So far, analyses of these models has been restricted to $\mathbf{H} = 0$, and to linear response to a weak $\mathbf{H}$. Here, we will look at the full non-linear response to a strong $\mathbf{H}$. It should be noted here that, in $d = 1$, closely related results can also be obtained by the bosonization technique of Chapter 14 [397], while making no reference to the rotor model—we will not follow such an approach here.

We prefer to begin our analysis by placing the continuum model $\mathcal{S}_n$ on a lattice at some short distance scale, and working with the discrete lattice Hamiltonian. This is the inverse of the mapping carried out in Chapter 5, and we therefore obtain the rotor model Hamiltonian H_R in (5.1):

$$H_R = \frac{Jg}{2} \sum_i \hat{\mathbf{L}}_i^2 - J \sum_{\langle ij \rangle} \hat{\mathbf{n}}_i \cdot \hat{\mathbf{n}}_j - \mathbf{H} \cdot \sum_i \hat{\mathbf{L}}_i. \tag{13.82}$$

The lattice sites in this rotor Hamiltonian are not to be identified with the lattice sites of H_S in (13.1); rather each rotor is an effective degree of freedom for a cluster of an even number of spins in the original model. Each such cluster will have a spin singlet ground state for $\mathbf{H} = 0$, as does the on-site Hamiltonian for each rotor in (13.82) - see (2.71). The rotor also has an infinite tower of states with increasing angular momentum in (2.71); in contrast a cluster of p Heisenberg spins with spin S can have a maximum total angular momentum pS. This difference will have some significant consequences for the topology of the phase diagram, but will leave many essential features unaltered–we will comment on this issue later.

We proceed to understanding the properties of H_R in the remainder of this section. The analysis will be quite similar to that discussed for the Boson Hubbard model in Chapter 10, and the results bear some similarity to those in Ref. [280]; indeed, we will find that the phase diagram of H_R is quite similar to that of H_B in (10.4), and the universality classes of the quantum phase transitions reduce either to the models studied in Part 2, or to those in Chapter 11. This similarity is not surprising at one level: the model H_R in the presence of a non-zero $\mathbf{H}$ only has a global U(1) symmetry corresponding to rotations about an axis parallel to the field (rotations about all other axes are not allowed by the non-zero $\mathbf{H}$), and the model H_B also has only a U(1) symmetry. (In the models considered in Ref [466], uniform moments appear spontaneously due to ferromagnetic exchange in a model with full O(3) symmetry, and this reasoning does not hold: however the similarity to H_B persists,

with many (but not all) quantum critical points belonging to the same universality classes as those of H_B.)

Most of the physics of H_R already becomes apparent in a mean-field theory similar to that in Section 10.1. As in (10.7), we make a mean-field ansatz for H_{MF} as the sum of single-site Hamiltonians with initially arbitrary variational parameters:

$$H_{MF} = \sum_i \left(\frac{Jg}{2} \hat{\mathbf{L}}_i^2 - \mathbf{H} \cdot \sum_i \hat{\mathbf{L}}_i - \mathbf{N} \cdot \hat{\mathbf{n}}_i \right). \tag{13.83}$$

Here the $\mathbf{N}$ are a set of three variational parameters which represent the effects of the exchange J with nearest neighbors in mean-field theory; they play a role similar to that of the complex number Ψ_B in Section 10.1. We have assumed that the $\mathbf{N}$ are site-independent and are therefore excluding the possibility of states with spatial structure: this is for simplicity and it is not difficult to extend our analysis to allow for broken translational symmetries in H_R.

Now the analysis proceeds as in Section 10.1: determine the ground state wavefunction of H_{MF}, and optimize the expectation value of H_R in this wavefunction towards variations in $\mathbf{N}$. This was done numerically, and leads to the phase diagram in Fig 13.4; we will discuss the properties of each of the phases in turn, and then consider the nature of the transitions between them.

13.4.1 Quantum paramagnet

The optimum value of the variational parameter is $\mathbf{N} = 0$. For this value, H_{MF} is exactly diagonalizable–the eigenstates are simply the rotor eigenstates $|\ell, m\rangle$ of (5.4) and have eigenvalues $Jg\ell(\ell+1)/2 - Hm$. The quantum paramagnet appears when parameters are such that the minimum energy state has $\ell = m = 0$: this happens for small H/J and large g. This quantum paramagnet is precisely the corresponding state of the rotor model studied in Part 2–the field $\mathbf{H}$ couples only to the total spin which is identically zero in the spin singlet ground state: as a result the wavefunction and all equal time correlations are unaffected by a non-zero $\mathbf{H}$. The energy of the spin triplet particle excitations does change as was shown in (5.6), but their wavefunctions also remain unaffected.

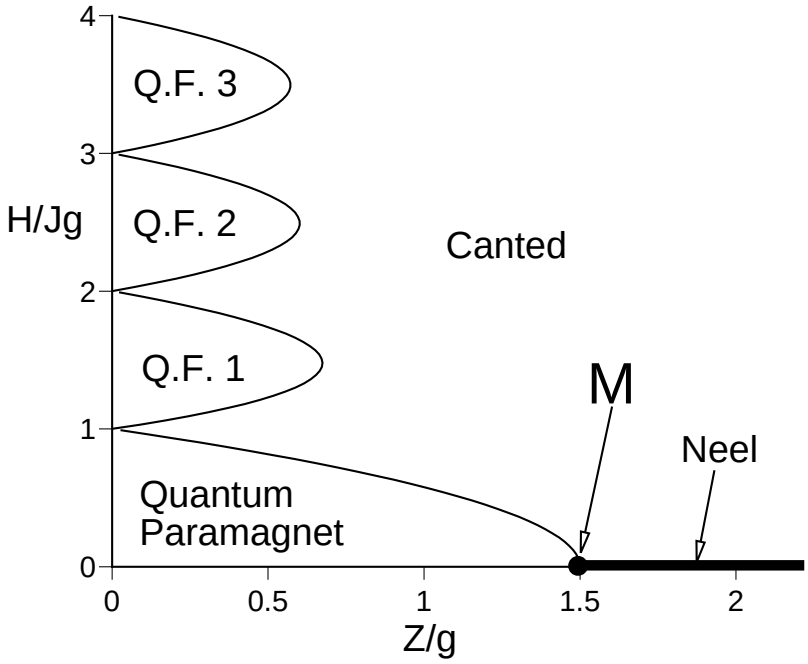

Fig. 13.4. Mean field phase diagram of H_R (in (13.82)), the O(3) quantum rotor model in a field $\mathbf{H}$. The notation Q.F. ℓ refers to a quantized ferromagnet with $\langle \hat{L}_z \rangle = \ell$. Compare with the phase diagram of the boson Hubbard model in Fig 10.1: in the latter case, there is no special meaning to the vertical coordinate = 0, and the vertical axis is unbounded below. The positions of the phase boundaries follow from (13.85). The multicritical point M is precisely the critical point of the O(3) quantum rotor model studied in Part 2.

13.4.2 Quantized ferromagnets

These phases also have $\mathbf{N} = 0$, and so the eigenenergies of H_{MF} are those listed above. The minimum energy state has $m = \ell$, and the different quantized ferromagnets are identified by the different positive integer values of ℓ as shown in Fig 13.4. The analogy between these phases and the Mott-insulating phases of Section 10.1 should be clear: the boson number n_0 corresponds to the integer ℓ. We argued in Section 10.1 that the quantization of n_0 was not an artifact of mean field theory but an exact statement about the full interacting model. Precisely the same arguments apply here to $\langle \hat{L}_z \rangle$ (we are assuming $\mathbf{H}$ is oriented in the z direction), as the total angular momentum in the z direction commutes with H_R. Such quantized ferromagnetic phases also appear in

the models of Ref [466] where ferromagnetism was induced by exchange interactions: in this case complete rotational symmetry of the underlying Hamiltonian implies that the there are gapless spin-wave excitations of the type considered in Section 13.2 with dispersion $\varepsilon_k = (\rho_s/M_0)k^2$. In the present model H_R the spin wave modes acquire a gap from the external field, and we have $\varepsilon_k = (\rho_s/M_0)k^2 + H$. In these respects these quantized ferromagnets are identical to the fully-polarized ferromagnets of Section 13.2: we simply have to set M_0 equal to the actual quantized value of the ground state magnetization density.

Let us also note some aspects of the interpretation of these quantized ferromagnet phases for underlying spin models like H_S. We noted above that each rotor was an effective degree of freedom for an even number, p, of Heisenberg spins. Such a cluster has maximum spin pS, and so the quantized ferromagnets with $\ell > pS$ clearly cannot exist, and are artifacts of the mapping to the rotor model which introduced an infinite tower of states on each site. Also, for some antiferromagnets, making clusters of p spins may involving reducing the symmetry of the underlying lattice. In this case the quantized ferromagnets with $0 < \ell < pS$ necessarily involve a spontaneously broken translational symmetry: each spin has an average fractional moment of ℓ/p and this can be quantized only if p spins spontaneously group together and carry a total moment ℓ together. This spontaneously broken symmetry will effect the critical theory of the transition out of the quantized phase, but we will not discuss this further here. Finally, the rotor with $\ell = p$ is a fully polarized ferromagnet which can exist without any broken translational symmetry.

It should also be noted that very similar considerations apply for the case of p odd: then we have to work with rotors which carry half integral angular momenta [489, 466].

13.4.3 Canted and Néel States

These states both have $\mathbf{N} \neq 0$, and are thus the analogs of the superfluid state of the boson model of Section 10.1. The Néel state occurs precisely at $\mathbf{H} = 0$, and the full rotational invariance of the Hamiltonian then implies that the direction of $\mathbf{N}$ is immaterial. The *canted* state occurs at non-zero $\mathbf{H}$. If we write $\mathbf{H} = H\mathbf{e}_z$, the numerical optimization of the mean-field Hamiltonian (13.83) shows that the vector $\mathbf{N}$ prefers to lie in the x-y plane; the direction within the plane is immaterial, reflecting the U(1) symmetry of the problem. This orientation of the Néel order parameter in a plane perpendicular to an applied uniform field is quite

generic, and the reasons for it will become more evident in Section 13.4.4 below. We choose $N_x \neq 0$ and $N_y = 0$. The resulting canted state is characterized by the non-zero expectation values

$$\langle \hat{n}_x \rangle = N_x/(JZ) \neq 0 \qquad \langle \hat{L}_z \rangle \neq 0, \tag{13.84}$$

and all other components of $\hat{\mathbf{n}}$ and $\hat{\mathbf{L}}$ have vanishing expectation values. The first relation in (13.84) should be compared with (10.9)–its origin is the same. Both non-zero expectation values in (13.84) vary continuously as a function of J, g or H, and nothing is pinned at a quantized value; as there is a non-zero, continuously varying ferromagnetic moment in the canted phase, this is an example of an *'unquantized' ferromagnet*. The results (13.84) also make the origin of term 'canted' clear, as shown in illustration within the canted region of Fig 13.6. In terms of the underlying Heisenberg spins, a non-zero $\langle \hat{n}_x \rangle$ implies antiferromagnetic ordering within the x direction in spin space, while a non-zero $\langle \hat{L}_z \rangle$ implies a uniform ferromagnetic moment in the z direction.

We show a plot of the H dependence of the $T = 0$ magnetization $\langle \hat{L}_z \rangle$ in Fig 13.5. Notice that there are plateaus in the magnetization while the system is in the quantum paramagnetic or quantized ferromagnetic phases. In between these phases is the canted phase, or the unquantized ferromagnet, in which the magnetization continuously interpolates between the quantized values.

The excitation structure of the canted phase is easy to work out. We simply follow the same procedure as that used to the Néel state in Section 5.1.2. Examining equations of the motion of small fluctuations about the ordered state one finds a gapless spin wave excitations with energy $\varepsilon_k \sim k$ corresponding to rotations of the $\hat{\mathbf{n}}$ in the x-y plane. For the case where the canted state appears in a model with full O(3) symmetry, there is an additional gapless mode with dispersion $\varepsilon_k \sim k^2$ [466].

The mean field boundary between the canted/Néel states and the quantized ferromagnets/quantum paramagnet can be computed analytically, using the same analysis leading up to (10.14) for the boson model. We expand the ground state energy of the quantized ferromagnet/quantum paramagnet in powers of N_x and demand that the co-efficient of the N_x^2 vanish. This leads to the analog of the condition $r = 0$ with the expressions (10.15), (10.16); in the present situation we find the condition

$$\frac{g}{Z} = \frac{\ell + 1}{(2\ell + 3)(\ell + 1 - H/Jg)} - \frac{\ell}{(2\ell + 1)(\ell - H/Jg)}$$

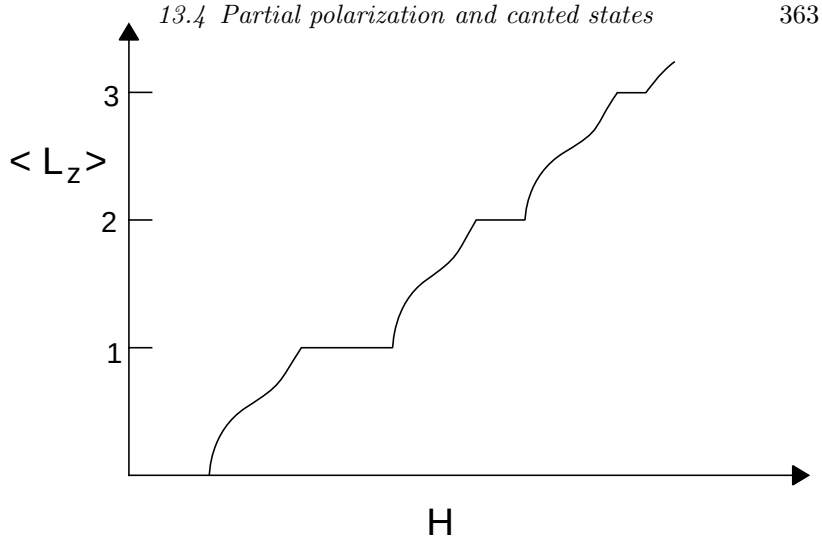

Fig. 13.5. Schematic of the magnetization, $\langle \hat{L}_z \rangle$, as a function of the field $\mathbf{H}$ for the rotor model (13.82). It is assumed that the value of Z/g in Fig 13.4 is small enough that a vertical line will intersect the Q.F. ℓ phases for $\ell \leq 3$. The magnetization is initially pinned at 0 when the system is in the quantum paramagnet, and is subsequently pinned at ℓ in the Q.F. phases. The magnetization interpolates between these plateaus in the canted or 'unquantized ferromagnet' phase.

$$\frac{1}{(2\ell+1)(2\ell+3)(\ell+1+H/Jg)} \tag{13.85}$$

for the instability of the quantized ferromagnet/quantum paramagnet with $\langle \hat{L}_z \rangle = \ell$ (the denominators in (13.85) are always positive over the range of applicability for a given value of ℓ). Simple application of (13.85) led to Fig 13.4.

An important feature of the above results deserves special mention. Notice that the only phase with a continually varying uniform magnetic moment (an unquantized ferromagnet) is the canted phase. This phase has a broken symmetry in the x-y plane and an associated gapless mode. This result is believed [466] to be a general principle: phases with continuously varying values of a ferromagnetic moment must have gapless spin modes in addition to the usual ferromagnetic spin-waves that are present for the case of a spontaneously generated moment; moreover, unlike the spin-waves, these gapless modes do not acquire a gap in the presence of a uniform field $\mathbf{H}$. In $d \geq 2$, for the rotor models considered here, the gapless modes are associated with the broken symmetry lead-

ing to canted order in such phases. In $d = 1$, the analysis in Chapter 11 shows that the order in the x-y plane becomes quasi long-range but the gapless mode survives.

(For completeness, we also note here another physical example of an unquantized ferromagnet: the Stoner ferromagnet [514] of an interacting Fermi gas, in which there are two Fermi surfaces, one each for up and down spins, with unequal Fermi wavevectors $k_{F\uparrow} \neq k_{F\downarrow}$. The values of $k_{F\uparrow}$ and $k_{F\downarrow}$ can vary continuously as the interaction strength is varied (provided they are both non-zero), and so can the mean magnetic moment. Consistent with the general principle above, in addition to the ferromagnetic spin-waves, this system has low energy spin-flip excitations at finite wave-vectors involving particle-hole pairs near the two Fermi surfaces.)

13.4.4 Zero temperature critical properties

It is clear that the $\mathbf{H} = 0$ transition between the quantum paramagnet and the Néel state is precisely the same as $N = 3$ model intensively studied in Part 2; this critical point is denoted M in Fig 13.4. We will show that the generic $\mathbf{H} \neq 0$ transition between the quantized ferromagnet/quantum paramagnet and the canted state is in the universality class of the dilute Bose gas field theory in (11.1), which was thoroughly studied in Chapter 11. We will do this by examining the line of second order transitions coming into the point M; the remaining portions of the phase boundary can be analyzed in a similar manner. It should also be noted that there are also special 'particle-hole' symmetric points at the tips of the lobes surrounding the quantized ferromagnet phases where the $z = 1$ theory of Part 2 will apply, just as was the case for the Boson Hubbard model in Sections 10.1 and 10.2.

The promised result is most easily established by using the 'soft-spin' theory of the point M studied in Chapter 8. In the presence of a field $\mathbf{H} = H\mathbf{e}_z$ the generalization of the $N = 3$ version of (8.2) is

$$\mathcal{S}_\phi = \int d^d x \int_0^{1/T} d\tau \left\{ \frac{1}{2} \left[(\partial_\tau \phi_x - iH\phi_y)^2 + (\partial_\tau \phi_y + iH\phi_x)^2 + (\partial_\tau \phi_z)^2 + c^2 (\nabla_x \vec{\phi})^2 + r\phi_\alpha^2 \right] + \frac{u_0}{4!} (\phi_\alpha^2)^2 \right\} \tag{13.86}$$

The uniform magnetic moment density is given by

$$\frac{1}{v} \langle \hat{L}_z \rangle = -\frac{\partial \mathcal{F}}{\partial H} \tag{13.87}$$

where v is the volume per rotor, and $\mathcal{F}$ is the free energy density associated with the action $\mathcal{S}_\phi$.

Let us first discuss the mean field properties of $\mathcal{S}_\phi$, obtained by minimizing the action, while ignoring all spatial and time dependence of ϕ_α; this will reproduce the structure in the vicinity of the point M in Fig 13.4 obtained earlier using the mean-field Hamiltonian (13.83). Notice that the components ϕ_x, ϕ_y have a quadratic term with coefficient $r - H^2$, while ϕ_z has the usual coefficient r; so ordering is preferred in the x-y plane, and this was the reason for the choice in the orientation of the $\mathbf{N}$ vector in Section 13.4.3. For $r - H^2 > 0$, the ground state has $\langle \phi_\alpha \rangle = 0$, and is therefore in the quantum paramagnetic phase. For $r - H^2 < 0$, the ground state has $\langle \phi_\alpha \rangle \neq 0$ and in the x-y plane. This is the C phase and the fields have the expectation values

$$\phi_\alpha = \left(\left(\frac{6(H^2 - r)}{u_0} \right)^{1/2}, 0, 0 \right) \qquad \frac{1}{v} \langle \hat{L}_z \rangle = \frac{6H(H^2 - r)}{u_0}, \quad (13.88)$$

or any rotation of ϕ_α in the $x - y$ plane. Notice that $\langle \hat{L}_z \rangle$ vanishes for $H = 0$, and therefore the line $r < 0$, $H = 0$ is the Néel state. The resulting mean field phase diagram is shown in Fig 13.6 and is identical to the vicinity of the point M in Fig 13.4. Let us focus on the vicinity of the generic transition between the quantum paramagnet and the canted phase: this corresponds to the regime $|r - H^2| \ll |r|$. In this region we can neglect ϕ_z fluctuations and focus only on the $\phi_x + i\phi_y$ which is undergoing Bose condensation. Further, the second-order time derivative in $\mathcal{S}_\phi$ can be dropped as the low energy properties are dominated by the more relevant first order time derivative that appears by expanding the first two terms in $\mathcal{S}_\phi$. Making these approximations, and defining

$$\Psi = \frac{\phi_x + i\phi_y}{\sqrt{H}}, \quad (13.89)$$

we see that $\mathcal{S}_\phi$ reduces to

$$\mathcal{S}_\Psi = \int d^2x \int_0^{1/T} d\tau \left[\Psi^* \frac{\partial \Psi}{\partial \tau} + \frac{c^2}{2H} |\nabla_x \Psi|^2 + \frac{(r - H^2)}{2H} |\Psi|^2 + \frac{u_0}{24H^2} |\Psi|^4 \right]. \quad (13.90)$$

This is precisely the theory (11.1), establishing the claim made at the beginning of this subsection.

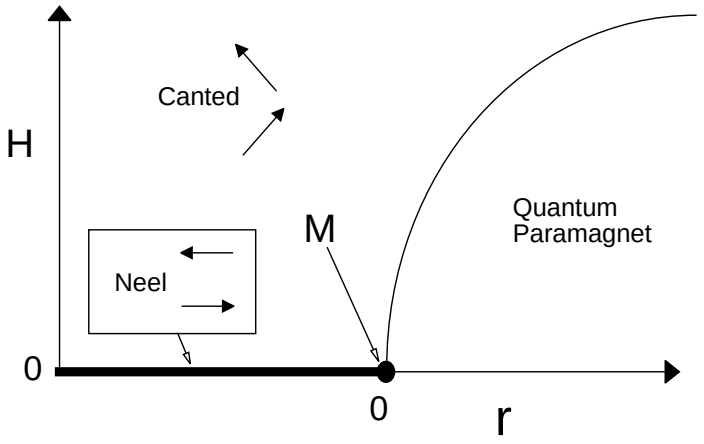

Fig. 13.6. Mean field phase diagram of $\mathcal{S}_\phi$ (in (13.86)) at $T = 0$. The arrows denote the relative orientation of the spins in the corresponding phases of double layer systems, which map onto the rotor model as discussed in Section 5.1.1.1; the field **H** is assumed to point towards the top of the page. The multi-critical point M is the $N = 3$ case of the quantum critical point studied in Part 2. Notice that the vicinity of M is similar to that in Fig 13.4.

13.5 Applications and extensions

There has been a great deal of theoretical work on possible quantum paramagnetic ground states of two dimensional, $S = 1/2$ Heisenberg antiferromagnets. On the square lattice, we have already noted the studies on the $J_1 - J_2$ and $J_1 - J_2 - J_3$ models which show clear evidence for the existence of a quantum paramagnetic ground state in a window around $J_2/J_1 \approx 0.5$, $J_3 = 0$. Some of these studies [186, 185, 375, 413, 480, 329, 309] also show reasonable evidence for the existence of columnar spin-Peierls order of the type discussed in Section 13.3.1.2 and shown in Fig 13.2, as was predicted from the Berry phase analyses of Refs [426, 427, 428, 464]. More recently, Zhitomirsky and Ueda [583] have suggested that the plaquette state in Fig 13.2 may be the lowest energy one: this possibility was not thoroughly tested in the earlier work. Experimental evidence for a direct transition from the Néel to the spin-Peierls state has appeared in recent work of the group led by S. E. Brown [96].

The weight of the evidence on the triangular lattice is that the model with only nearest neighbor interactions has long range Néel order of

the type shown in Fig 13.3 [100, 306, 51]; other types of magnetic order appear upon including further neighbor exchanges [321]. However, the introduction of multiple spin ring exchanges can induce quantum paramagnetic ground states [370], and these are candidates for exhibiting deconfined spinon excitations in two dimensions. The latter case of multiple spin exchange appears to have an experimental realization in experiments on an adsorbed ^{3}He layer on graphite [437].

The nearest neighbor $S = 1/2$ antiferromagnet on the kagome lattice has also been intensively studied: here it is virtually certain that the ground state is a quantum paramagnet with a gap towards excitations with non-zero spin. However, there appear to be a large number of low-lying, singlet excitations. These could possibly be described by an effective quantum dimer model [436] and arguments have been advanced [444] that this model should have a gap on the kagome lattice. The current situation, along with earlier references to the literature, has been discussed by Waldtmann *et al.* [557].

The most precise study of the quantum critical point between an ordered Néel state and a quantum paramagnet has been carried out by Troyer *et al.* [531] on a depleted square lattice. All universal properties are in agreement with those of the O(3) quantum rotor model of Part 2, supporting the irrelevancy of the Berry phase terms, discussed in Section 13.3.1.2, for the critical phenomena.

An important experimental candidate for a gapped quantum paramagnetic ground state in two dimensions in CaV_4O_9. The experimental measurements [520] clearly indicate the presence of a spin gap, but there remains a debate upon the nature of the microscopic spin Hamiltonian needed to explain the observations [188, 408, 288].

Many of the spin-gapped insulators found in recent years, including the spin-ladder compounds, can be naturally decomposed into pairs of spins without reducing the symmetries of the lattice, as for the model of Section 5.1.1.1. Microscopic studies [198, 391, 392, 409, 308] of such systems can be performed using the 'bond boson' method [459] in which triplet and singlet bosons reside on the bonds connecting the two spins in a pair.

The analyses of Section 13.4 should make it clear that the dilute Bose gas quantum critical point of Chapter 11 describes the closing of a spin gap of an antiferromagnet by a strong external magnetic field [478, 6, 7, 536, 503, 467, 94]. This critical point has been intensively studied recently in spin ladder organic compound $Cu_2(C_5H_{12}N_2)_2Cl_4$ [82, 83, 84, 225, 146]. The onset of magnetization plateaus at a finite field (as in

Fig 13.5) is also described by the same quantum critical point, and such plateaus have been observed recently in experiments on one-dimensional spin chains [383, 493].

A novel realization of the $d = 2$ continuum quantum ferromagnets of Section 13.2 is provided by magnetization studies of single layer quantum Hall systems at filling factor $\nu = 1$ [501, 155, 286, 287]. These are electronic systems with a gap towards charged excitations, and a strong ferromagnetic exchange between the electronic spins. As a result, the low-lying spin excitations are well described by the continuum theory (13.32). The magnetization of this system for different T and H has been measured in NMR [40] and optical [14, 350] experiments, and the results have been interpreted by computations on (13.32) [27, 429, 524, 240].

Exciting recent developments have appeared in studies of double layer quantum Hall systems, when two single layer systems in a ferromagnetic quantum Hall state with a charge gap, are brought close to each other [410, 401, 474, 402]. There is an antiferromagnetic exchange pairing between the layers [581], which suggests that we may consider the two layers to be similar to the two sublattices of an antiferromagnet, and that there is an effective rotor model description of the spin excitations. Indeed, it has been argued [128, 129] that the system maps precisely onto the model studied in Section 13.4. Detailed light scattering studies have mapped out the phase diagram of the system [402], and the results are consistent with Figs 13.4 and 13.6. Specific quantitative predictions for quantum critical behavior have been made in Refs [128, 129, 532, 355, 456], and these and dynamical results like those in Section 8.3 could be tested in future experiments.

Annales Henri Poincare 4, 559 (2003)

Field theories of paramagnetic Mott insulators

Subir Sachdev
Department of Physics, Yale University,
P.O. Box 208120, New Haven CT 06520-8120

Proceedings of the International Conference on
Theoretical Physics, Paris, UNESCO, 22-27 July 2002.

Abstract

This is a summary of a central argument in recent review articles by the author (Physica A **313**, 252 (2002), Annals of Physics **303**, 226 (2003), and Rev. Mod. Phys, July 2003). An effective field theory is derived for the low energy spin singlet excitations in a paramagnetic Mott insulator with collinear spin correlations.

1 INTRODUCTION

In a recent article [1](intended for an audience of experimentalists), the author has reviewed arguments that many aspects of the physics of the cuprate superconductors can be understood by using their proximity to paramagnetic Mott insulators. Further, a distinction was made between Mott insulators with collinear and non-collinear spin correlations, and it was argued that current experimental evidence suggests that we need only consider the collinear class. A phenomenological description of the ground states and excitations of these classes of Mott insulators was provided, along with a discussion of their experimental implications. A more technical discussion (intended for theorists) of such insulators, along with a description of the effective field theories which describe their low energy properties appears in Ref. [2, 3]. Here, we briefly recall the derivation and properties of the effective field theory of Mott insulators with *collinear* spin correlations, which is expressed in terms of a compact U(1) gauge field. The non-collinear class leads naturally

to a Z_2 gauge theory, but we will not consider it here. The reader is referred to these previous reviews [1, 2, 3] for complete citations to the literature.

2 Compact U(1) gauge theory of Mott insulators

We focus on Mott insulators on a d dimensional bipartite lattice of sites j. The SU(2) spin operator $\mathbf{S}_j$ on site j at imaginary time τ can be written as

$$\mathbf{S}_j(\tau) = \eta_j S \mathbf{n}(r_j, \tau); \tag{1}$$

here $\eta_j = \pm 1$ on the two sublattices, r_j is the spatial co-ordinate of site j, $\mathbf{n}$ is a unit length vector in spin space, and S is the (integer or half-odd-integer) angular momentum of each spin. The antiferromagnetic exchange interaction between near neighbor spins implies that $\mathbf{n}(r_j, \tau)$ will be a slowly varying function of its spacetime arguments. A standard analysis of the coherent state path integral of over the SU(2) $\mathbf{S}_j$ spins shows that the low energy quantum fluctuations are described by the following partition function

$$\begin{aligned} \mathcal{Z} &= \int \mathcal{D}\mathbf{n}(r,\tau)\delta(\mathbf{n}^2(r,\tau)-1)\exp\Bigg[-iS\sum_j \eta_j \int d\tau \mathcal{A}_\tau(\mathbf{n}(r_j,\tau)) \\ &\quad - \frac{1}{2gc}\int d^d r d\tau \left((\partial_\tau \mathbf{n})^2 + c^2(\nabla_r \mathbf{n})^2\right)\Bigg], \end{aligned} \tag{2}$$

where c is the spin-wave velocity, and g is a coupling constant which controls the strength of the quantum fluctuations. Excluding the first Berry phase term, this is the action of the O(3) non-linear sigma model in $d+1$ spacetime dimensions. Here we are primarily interested in the consequences of the Berry phases: $\mathcal{A}_\tau(\mathbf{n}(\tau))d\tau$ is defined to be the oriented area of the spherical triangle defined by $\mathbf{n}(\tau)$, $\mathbf{n}(\tau + d\tau)$, and an arbitrary reference point $\mathbf{n}_0$ (which is usually chosen to be the north pole).

The theory (2) can be considered to be the "minimal model" of antiferromagnets. In dimensions $d > 1$ it has at least two phases: at small g there is the conventional magnetically ordered "Néel" phase with $\langle \mathbf{n} \rangle \neq 0$, while at large g there is a "quantum disordered" paramagnetic phase which preserves spin rotation invariance with $\langle \mathbf{n} \rangle = 0$. We are especially interested here in the nature of this paramagnetic state. In this section, we will manipulate

$\mathcal{Z}$ in this large g regime, and derive an alternative formulation which allows easier computation of the integral over the Berry phases.

The key to an analysis of the large g regime is a better understanding of the nature of $\mathcal{A}_\tau$. We will see that $\mathcal{A}_\tau$ behaves in many respects like the time-component of a compact U(1) gauge field, and indeed, this accounts for the suggestive notation. All physical results should be independent of the choice of the reference point $\mathbf{n}_0$, and it is easy to see by drawing triangles on the surface of a sphere that changes in $\mathbf{n}_0$ amount to gauge transformations of $\mathcal{A}_\tau$. If we change $\mathbf{n}_0$ to $\mathbf{n}_0'$, then the resulting $\mathcal{A}_\tau'$ is related to $\mathcal{A}_\tau$ by

$$\mathcal{A}_\tau' = \mathcal{A}_\tau - \partial_\tau \phi(\tau) \tag{3}$$

where $\phi(\tau)$ measures the oriented area of the spherical triangle defined by $\mathbf{n}(\tau)$, $\mathbf{n}_0$, and $\mathbf{n}_0'$. Furthermore, as we will discuss more completely below, the area of any spherical triangle is uncertain modulo 4π, and this accounts for the 'compactness' of the U(1) gauge theory.

We proceed with our analysis of $\mathcal{Z}$. First, we discretize the gradient terms of the O(3) sigma model. We will limit our considerations here to antiferromagnets on d dimensional cubic lattices, but similar considerations apply to other bipartite lattices. We also discretize the imaginary time direction, and (by a slight abuse of notation) use the same index j to refer to the sites of a $d+1$ dimensional cubic lattice in spacetime. On such a lattice we can rewrite (2) as

$$Z = \int \prod_j d\mathbf{n}_j \delta(\mathbf{n}_j^2 - 1) \exp\left(\frac{1}{2g} \sum_{j,\mu} \mathbf{n}_j \cdot \mathbf{n}_{j+\hat{\mu}} - iS \sum_j \eta_j \mathcal{A}_{j\tau} \right), \tag{4}$$

where the sum over μ extends over the $d+1$ spacetime directions. We have also dropped unimportant factors of the lattice spacing and the spin-wave velocity in (4).

As noted above, we are especially interested here in the large g regime where there are strong fluctuations of the $\mathbf{n}_j$. There are strong cancellations from the Berry phases between different spin configurations in this regime, and so the second term in Z has to be treated with great care. We will do this by promoting the field $\mathcal{A}_{j\mu}$ to an independent degree of freedom, while integrating out the $\mathbf{n}_j$. Notice that we have now introduced all $d+1$ components of the compact U(1) gauge field with the index μ, while only the $\mu = \tau$ component appears explicitly in (4). The remaining components

appear naturally as suitable degrees of freedom when we integrate the $\mathbf{n}_j$ out. Formally, the integration over the $\mathbf{n}_j$ can be done by introducing new 'dummy' variables $A_{j\mu}$ and rewriting (4) by introducing factors of unity on each link; this leads to

$$\begin{aligned} Z &= \int \prod_{j\mu} dA_{j\mu} \exp\left(-i2S \sum_j \eta_j A_{j\tau}\right) \int \prod_j d\mathbf{n}_j \delta(\mathbf{n}_j^2 - 1) \delta(\mathcal{A}_{j\mu}/2 - A_{j\mu}) \\ &\qquad \times \exp\left(\frac{1}{2g} \sum_{j,\mu} \mathbf{n}_j \cdot \mathbf{n}_{j+\hat{\mu}}\right) \\ &= \int \prod_{j\mu} dA_{j\mu} \exp\left(-\mathcal{S}_A(A_{j\mu}) - i2S \sum_j \eta_j A_{j\tau}\right). \end{aligned} \tag{5}$$

In the first expression, if the integral over the $A_{j\mu}$ is performed first, we trivially return to (4); however, in the second expression we perform the integral over the $\mathbf{n}_j$ variables first, at the cost of introducing an unknown effective action $\mathcal{S}_A$ for the $A_{j\mu}$. In principle, evaluation of $\mathcal{S}_A$ may be performed order-by-order in a "high temperature" expansion in $1/g$: we match correlators of the $A_{j\mu}$ flux with those of the $\mathcal{A}_{j\mu}$ flux evaluated in the integral over the $\mathbf{n}_j$ with positive weights determined only by the $1/g$ term in (4). Rather than undertaking this laborious calculation, we can guess essential features of the effective action $\mathcal{S}_A$ from some general constraints. First, correlations in the $\mathbf{n}_j$ decay exponentially rapidly for large g (with a correlation length $\sim 1/\ln(g)$), and so $\mathcal{S}_A$ should be local. Second, it should be invariant under the lattice form of the gauge transformation (3)

$$A'_{j\mu} = A_{j\mu} - \Delta_\mu \phi_j/2 \tag{6}$$

associated with the change in the reference point on the unit sphere from $\mathbf{n}_0$ to $\mathbf{n}'_0$, with ϕ_j equal to the area of the spherical triangle formed by $\mathbf{n}_j$, $\mathbf{n}_0$ and $\mathbf{n}'_0$. Finally the area of any triangle on the sphere is uncertain modulo 4π and so the effective action should be invariant under

$$A_{j\mu} \to A_{j\mu} + 2\pi. \tag{7}$$

The simplest local action which is invariant under (6) and (7) is that of *compact U(1) quantum electrodynamics* and so we have

$$Z = \int \prod_{j\mu} dA_{j\mu} \exp\left(\frac{1}{e^2} \sum_\square \cos\left(\Delta_\mu A_{j\nu} - \Delta_\nu A_{j\mu}\right) - i2S \sum_j \eta_j A_{j\tau}\right), \tag{8}$$

for large g; comparison with the large g expansion shows that the coupling $e^2 \sim g^2$. In (8), Δ_μ is the discrete lattice derivative along the μ direction, and the sum over $\Box$ extends over all plaquettes of the $d+1$ dimensional cubic lattice—both notations are standard in the lattice gauge theory literature.

The first term in the action (8) is, of course, the standard 'Maxwell' term of a compact U(1) gauge field. In this language, the Berry phase has the interpretation of a $\int J_\mu A_\mu$ coupling to a fixed matter field with 'current' $J_\mu = 2S\delta_{\mu\tau}$. This corresponds to static matter with charges $\pm 2S$ on the two sublattices. It is this matter field which will crucially control the nature of the ground state.

The remaining analysis of Z depends upon the spatial dimensionality d. In $d = 1$, a dual model of (8) is solvable, and the results are in complete accord with those obtained earlier by Bethe ansatz and bosonization analyses of spin chains. We will consider the $d = 2$ case in the section below. There has been relatively little discussion of the $d = 3$ case (which exhibits both confining and deconfining phases of the gauge theory), and this remains an important avenue for future research.

3 Duality mapping in $d = 2$

As is standard in duality mappings, we first rewrite the partition function in $2 + 1$ spacetime dimensions by replacing the cosine interaction in (8) by a Villain sum over periodic Gaussians:

$$Z = \sum_{\{q_{\bar{j}\mu}\}} \int \prod_{j\mu} dA_{j\mu} \exp\left(-\frac{1}{2e^2} \sum_{\Box} \left(\epsilon_{\mu\nu\lambda}\Delta_\nu A_{j\lambda} - 2\pi q_{\bar{j}\mu}\right)^2 - i2S \sum_j \eta_j A_{j\tau} \right), \tag{9}$$

where $\epsilon_{\mu\nu\lambda}$ is the total antisymmetric tensor in three dimensions, and the $q_{\bar{j}\mu}$ are integers on the links of the *dual* cubic lattice, which pierce the plaquettes of the direct lattice. Throughout this subsection we will use the index $\bar{j}$ to refer to sites of this dual lattice, while j refers to the direct lattice on sites on which the spins are located.

We will now perform a series of exact manipulations on (9) which will lead to a dual *interface* model [4, 5]. This dual model has only positive weights—this fact, of course, makes it much more amenable to a standard statistical analysis. This first step in the duality transformation is to rewrite

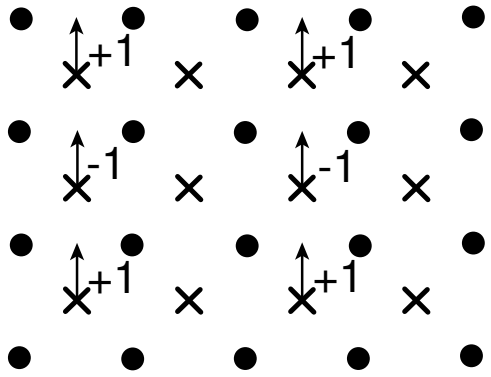

Figure 1: Specification of the non-zero values of the fixed field $a^0_{\bar{j}\mu}$. The circles are the sites of the direct lattice, j, while the crosses are the sites of the dual lattice, $\bar{j}$; the latter are also offset by half a lattice spacing in the direction out of the paper (the $\mu = \tau$ direction). The $a^0_{\bar{j}\mu}$ are all zero for $\mu = \tau, x$, while the only non-zero values of $a^0_{\bar{j}y}$ are shown above. Notice that the a^0 flux obeys (11).

(9) by the Poisson summation formula:

$$\sum_{\{q_{\bar{j}\mu}\}} \exp \left(-\frac{1}{2e^2} \sum_{\Box} \left(\epsilon_{\mu\nu\lambda} \Delta_\nu A_{j\lambda} - 2\pi q_{\bar{j}\mu} \right)^2 \right) = \sum_{\{a_{\bar{j}\mu}\}} \exp \left(-\frac{e^2}{2} \sum_{\bar{j}} a^2_{\bar{j}\mu} - i \sum_{\Box} \epsilon_{\mu\nu\lambda} a_{\bar{j}\mu} \Delta_\nu A_{j\lambda} \right), \quad (10)$$

where $a_{\bar{j}\mu}$ (like $q_{\bar{j}\mu}$) is an integer-valued vector field on the links of the dual lattice (here, and below, we drop overall normalization factors in front of the partition function). Next, we write the Berry phase in a form more amenable to duality transformations. Choose a 'background' $a_{\bar{j}\mu} = a^0_{\bar{j}}$ flux which satisfies

$$\epsilon_{\mu\nu\lambda} \Delta_\nu a^0_{\bar{j}\lambda} = \eta_j \delta_{\mu\tau}, \quad (11)$$

where j is the direct lattice site in the center of the plaquette defined by the curl on the left-hand-side. Any integer-valued solution of (11) is an acceptable choice for $a^0_{\bar{j}\mu}$, and a convenient choice is shown in Fig 1. Using (11) to rewrite the Berry phase in (9), applying (10), and shifting $a_{\bar{j}\mu}$ by the

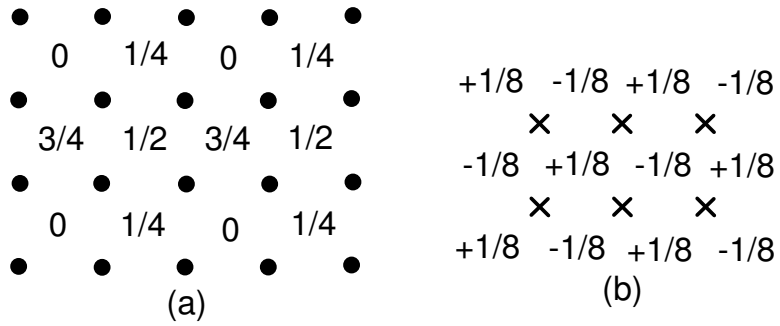

Figure 2: Specification of the non-zero values of the fixed fields (a) $\mathcal{X}_{\bar{\jmath}}$ and (b) $\mathcal{Y}_{j\mu}$ introduced in (14). The notational conventions are as in Fig 1. Only the $\mu = \tau$ components of $\mathcal{Y}_{j\mu}$ are non-zero, and these are shown in (b).

integer $2Sa^0_{\bar{\jmath}\mu}$, we obtain a new exact representation of Z in (9):

$$Z = \sum_{\{a_{\bar{\jmath}\mu}\}} \int \prod_{j\mu} dA_{j\mu} \exp\left(-\frac{e^2}{2} \sum_{\bar{\jmath},\mu} (a_{\bar{\jmath}\mu} - 2Sa^0_{\bar{\jmath}\mu})^2 - i \sum_{\square} \epsilon_{\mu\nu\lambda} a_{\bar{\jmath}\mu} \Delta_\nu A_{j\lambda} \right). \tag{12}$$

The integral over the $A_{j\mu}$ can be performed independently on each link, and its only consequence is the imposition of the constraint $\epsilon_{\mu\nu\lambda}\Delta_\nu a_{\bar{\jmath}\lambda} = 0$. We solve this constraint by writing $a_{\bar{\jmath}\mu}$ as the gradient of a integer-valued 'height' $h_{\bar{\jmath}}$ on the sites of the dual lattice, and so obtain

$$Z = \sum_{\{h_{\bar{\jmath}}\}} \exp\left(-\frac{e^2}{2} \sum_{\bar{\jmath},\mu} (\Delta_\mu h_{\bar{\jmath}} - 2Sa^0_{\bar{\jmath}\mu})^2 \right). \tag{13}$$

This is the promised 2+1 dimensional interface, or height, model in almost its final form.

The physical properties of (13) become clearer by converting the "frustration" $a^0_{\bar{\jmath}\mu}$ in (13) into offsets for the allowed height values. This is done by decomposing $a^0_{\bar{\jmath}\mu}$ into curl and divergence free parts and writing it in terms of new fixed fields, $\mathcal{X}_{\bar{\jmath}}$ and $\mathcal{Y}_{j\mu}$ as follows:

$$a^0_{\bar{\jmath}\mu} = \Delta_\mu \mathcal{X}_{\bar{\jmath}} + \epsilon_{\mu\nu\lambda}\Delta_\nu \mathcal{Y}_{j\lambda}. \tag{14}$$

The values of these new fields are shown in Fig 2. Inserting (14) into (13),

we can now write the height model in its simplest form [4]

$$Z_h = \sum_{\{H_{\bar{\jmath}}\}} \exp\left(-\frac{e^2}{2}\sum_{\bar{\jmath}} \left(\Delta_\mu H_{\bar{\jmath}}\right)^2\right), \tag{15}$$

where

$$H_{\bar{\jmath}} \equiv h_{\bar{\jmath}} - 2S\mathcal{X}_{\bar{\jmath}} \tag{16}$$

is the new height variable we shall work with. Notice that the $\mathcal{Y}_{j\mu}$ have dropped out, while the $\mathcal{X}_{\bar{\jmath}}$ act only as fractional offsets (for S not an even integer) to the integer heights. From (16) we see that for half-odd-integer S the height is restricted to be an integer on one of the four sublattices, an integer plus 1/4 on the second, an integer plus 1/2 on the third, and an integer plus 3/4 on the fourth; the fractional parts of these heights are as shown in Fig 2a; the steps between neighboring heights are always an integer plus 1/4, or an integer plus 3/4. For S an odd integer, the heights are integers on one square sublattice, and half-odd-integers on the second sublattice. Finally for even integer S the offset has no effect and the height is an integer on all sites. We discuss these classes of S values in turn in the following subsections.

3.1 S even integer

In this case the offsets $2S\mathcal{X}_{\bar{\jmath}}$ are all integers, and (15) is just an ordinary three dimensional height model which has been much studied in the literature. Unlike the two-dimensional case, three-dimensional height models generically have no roughening transition, and the interface is always smooth. With all heights integers, the smooth phase breaks no lattice symmetries. So square lattice antiferromagnets with S even integer can have a paramagnetic ground state with a spin gap and no broken symmetries. This is in accord with the exact ground state for a $S = 2$ antiferromagnet on the square lattice found by Affleck *et al.*, the AKLT state [6].

3.2 S half-odd-integer

Now the heights of the interface model can take four possible values, which are integers plus the offsets on the four square sublattices shown in Fig 2a. As in Section 3.1, the interface is always smooth *i.e.* any state of (15) has

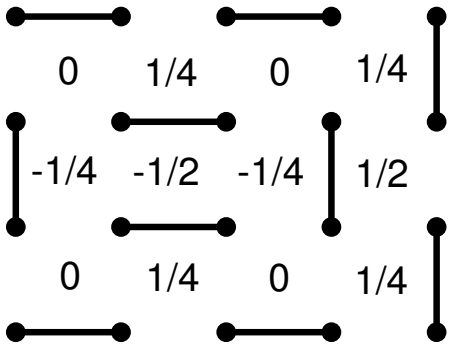

Figure 3: Mapping between the quantum dimer model and the interface model Z in (15). Each dimer on the direct lattice is associated with a step in height of $\pm 3/4$ on the link of the dual lattice that crosses it. All other height steps are $\pm 1/4$. Each dimer represents a singlet valence between the sites, as in Fig 2.

a fixed average interface height $\sum_{\bar{\jmath}} \langle H_{\bar{\jmath}} \rangle$, and *any* well-defined value for this average height breaks the uniform shift symmetry of the height model under which $H_{\bar{\jmath}} \to H_{\bar{\jmath}} \pm 1$. After accounting for the height offsets, we will see below that any smooth interface must also break a lattice symmetry with the development of *bond order*: this allows a number of distinct spin gap ground states of the lattice antiferromagnet.

It is useful, first, to obtain a simple physical interpretation of the interface model in the language of the $S = 1/2$ antiferromagnet [7]. From Fig 2a it is clear that nearest neighbor heights can differ either by $1/4$ or $3/4$ (modulo integers). To minimize the action in (15), we should choose the interface with the largest possible number of steps of $\pm 1/4$. However, the interface is frustrated, and it is not possible to make all steps $\pm 1/4$ and at least a quarter of the steps must be $\pm 3/4$. Indeed, there is a precise one-to-one mapping between interfaces with the minimal number of $\pm 3/4$ steps (we regard interfaces differing by a uniform integer shift in all heights as equivalent) and the dimer coverings of the square lattice: the proof of this claim is illustrated in Fig 3. We identify each dimer with a singlet valence bond between the spins (the ellipses in Fig 2), and so each interface corresponds to a quantum state with each spin locked in the a singlet valence bond with a particular nearest neighbor. Fluctuations of the interface in imaginary time between such configurations correspond to quantum tunneling events between such dimer states, and an effective Hamiltonian for this is provided by the quantum

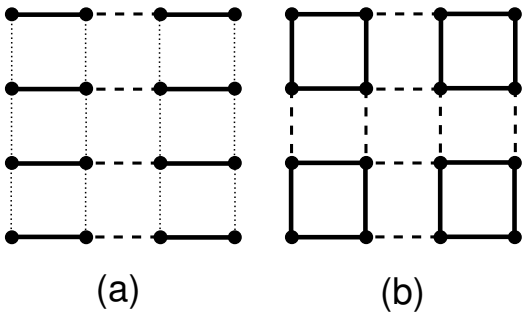

Figure 4: Sketch of the two simplest possible states with bond order for $S = 1/2$ on the square lattice: (a) the columnar spin-Peierls states, and (b) plaquette state. The different values of the $\langle \mathbf{S}_i \cdot \mathbf{S}_j \rangle$ on the links are encoded by the different line styles. Both states are 4-fold degenerate; an 8-fold degenerate state, with superposition of the above orders, also appears as a possible ground state of the generalized interface model.

dimer model [8].

The nature of the possible smooth phases of the interface model are easy to determine from the above picture and by standard techniques from statistical theory [4, 7]. Interfaces with average height $\langle H_{\bar{\jmath}} \rangle = 1/8, 3/8, 5/8, 7/8$ (modulo integers) correspond to the four-fold degenerate bond-ordered states in Fig 4a, while those with $\langle H_{\bar{\jmath}} \rangle = 0, 1/4, 1/2, 3/4$ (modulo integers) correspond to the four-fold degenerate plaquette bond-ordered states in Fig 4b. All other values of $\langle H_{\bar{\jmath}} \rangle$ are associated with eight-fold degenerate bond-ordered states with a superposition of the orders in Fig 4a and b.

Support for the class of bond-ordered states described above has appeared in a number of numerical studies of $S = 1/2$ antiferromagnets in $d = 2$ which have succeeded in moving from the small g Néel phase to the large g paramagnet. These include studies on the honeycomb lattice [9], on the planar pyrochlore lattice [10], on square lattice models with ring-exchange and easy-plane spin symmetry [12], and square lattice models with SU(N) symmetry [14].

3.3 S odd integer

This case is similar to that S half-odd-integer, and we will not consider it in detail. The Berry phases again induce bond order in the spin gap state, but

this order need only lead to a two-fold degeneracy.

4 Conclusions

The primary topic discussed in this paper has been the effective field theory of paramagnetic Mott insulators with collinear spin correlations. This field theory is the compact U(1) gauge theory in (8), and applies in all spatial dimensions. We also reviewed duality mappings of (8) which are special to $d = 2$ spatial dimensions, and mapped the theory onto the interface model (15). Finally, we reiterate that paramagnetic Mott insulators with non-collinear spin correlations are described by a Z_2 gauge theory which has not been presented here.

References

[1] S. Sachdev, Rev. Mod. Phys. July 2003, cond-mat/0211005.

[2] S. Sachdev, Physica A **313**, 252 (2002).

[3] S. Sachdev, Annals of Physics **303**, 226 (2003).

[4] N. Read and S. Sachdev, Phys. Rev. Lett. **62**, 1694 (1989); Phys. Rev. B **42**, 4568 (1990).

[5] E. Fradkin and S. A. Kivelson, Mod. Phys. Lett. B **4**, 225 (1990).

[6] I. Affleck, T. Kennedy, E. H. Lieb, and H. Tasaki, Phys. Rev. Lett. **59**, 799 (1987).

[7] W. Zheng and S. Sachdev, Phys. Rev. B **40**, 2704 (1989).

[8] D. Rokhsar and S. A. Kivelson, Phys. Rev. Lett. **61**, 2376 (1988)

[9] J.-B. Fouet, P. Sindzingre, and C. Lhuillier, Eur. Phys. J. B **20**, 241 (2001); duality mapping on the honyecomb lattice appears in Ref. [4].

[10] J.-B. Fouet, M. Mambrini, P. Sindzingre, and C. Lhuillier, Phys. Rev. B **67**, 054411 (2003); duality mapping for a lattice with the symmetry of the planar pyrochore is in Ref. [11], with a prediction for the bond order observed.

[11] C.-H. Chung, J. B Marston, and S. Sachdev, Phys. Rev. B **64**, 134407 (2001).

[12] A. W. Sandvik, S. Daul, R. R. P. Singh, and D. J. Scalapino, Phys. Rev. Lett., **89**, 247201 (2002); duality mapping on spin models with with easy plane symmetry is in Ref. [13].

[13] K. Park and S. Sachdev, Phys. Rev. B **65**, 220405 (2002).

[14] K. Harada, N. Kawashima, and M. Troyer, Phys. Rev. Lett. **90**, 117203 (2003); the theory (15) applies unchanged to SU(N) antiferromagnets.